Project Report
ATC-209

Assessment of the Weather Detection Capability of an Airport Surveillance Radar with Solid-State Transmitter

M.E. Weber
S.W. Troxel

24 February 1994

Lincoln Laboratory
MASSACHUSETTS INSTITUTE OF TECHNOLOGY
LEXINGTON, MASSACHUSETTS

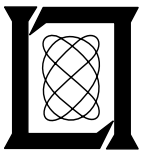

Prepared for the Federal Aviation Administration,
Washington, D.C. 20591

TECHNICAL REPORT STANDARD TITLE PAGE

1. Report No.	2. Government Accession No.	3. Recipient's Catalog No.
ATC-209	DOT/FAA/RD-94/1	

4. Title and Subtitle	5. Report Date
Assessment of the Weather Detection Capability of an Airport Surveillance Radar with Solid-State Transmitter	24 February 1994
	6. Performing Organization Code

7. Author(s)	8. Performing Organization Report No.
Mark E. Weber and Seth W. Troxel	ATC-209

9. Performing Organization Name and Address	10. Work Unit No. (TRAIS)
Lincoln Laboratory, MIT P.O. Box 73 Lexington, MA 02173-9108	11. Contract or Grant No. DTFA01-93-Z-02012

12. Sponsoring Agency Name and Address	13. Type of Report and Period Covered
Department of Transportation Federal Aviation Administration Systems Research and Development Service Washington, DC 20591	Project Report
	14. Sponsoring Agency Code

15. Supplementary Notes

This report is based on studies performed at Lincoln Laboratory, a center for research operated by Massachusetts Institute of Technology under Air Force Contract F19628-90-C-0002.

16. Abstract

The Federal Aviation Administration may acquire a new Airport Surveillance Radar ASR-11 to replace aging ASR-7s and ASR-8s with a digital terminal radar consistent with Advanced Automation System requirements. A survey of the radar manufacturing industry suggests that a solid-state transmitter will likely be a component of this radar. The ASR-11 will feature a digital weather processing channel to measure and display six calibrated levels of precipitation reflectivity. An additional weather surveillance goal is the capability to support detection of low altitude wind shear phenomena. Use of a low peak power, solid-state transmitter and associated pulse compression technology raises several issues with repect to the capability of ASR-11 to meet these weather measurement objectives:

1. ASR-11 sensitivity will be degraded by approximately 16 to 20 dB relative to the Klystron-based ASR-9 at short range. This results because it is not feasible to use pulse compression waveforms to compensate for low peak transmitted power at short range;

2. Stability of a solid-state ASR-11 transmitter may significantly exceed that of previous vacuum tube ASR transmitters. Increased clutter suppression capability associated with this enhanced stability could partially offset the reduced sensitivity of ASR-11 in meeting weather detection goals;

3. Pulse compression range sidelobes may result in "ghost" images of actual weather features, displaced in range by as much as 10 km. In some circumstances, these could result in false indications of operationally significant weather features such as thunderstorm-induced gust fronts.

We examine these issues through straightforward analyses and simulation. Our assessment depends heavily on Doppler weather radar measurements of thunderstorms and associated wind shear phenomena obtained with Lincoln Laboratory's Terminal Doppler Weather Radar and ASR-9 testbeds. Overall, our assessment indicates that a solid-state transmitter ASR-11 can provide six-level weather reflectivity data with accuracy comparable to that of the ASR-9. Detection of low altitude wind shear phenomena using a solid-state transmitter ASR is more problematic. Reduced sensitivity at short range—the range interval of primary operational concern for an on-airport ASR—results in significant degradation of its capability to measure the reflectivity and Doppler velocity signatures associated with gust fronts and "dry" microbursts. This degradation is not offset by the enhanced clutter suppression capability provided by a solid-state transmitter. Although pulse compression range sidelobes do not appear to be a major issue if they are held to the -55 dB level, simulations are presented where range sidelobes result in a false gust front wind shear signature.

17. Key Words		18. Distribution Statement
Airport Surveillance Radar	pulse compression	This document is available to the public through the National Technical Information Service, Springfield, VA 22161.
Solid-State Transmitter	wind shear	
weather surveillance		

19. Security Classif. (of this report)	20. Security Classif. (of this page)	21. No. of Pages	22. Price
Unclassified	Unclassified	71	

ABSTRACT

The Federal Aviation Administration may acquire a new Airport Surveillance Radar–ASR-11–to replace aging ASR-7s and ASR-8s with a digital terminal radar consistent with Advanced Automation System requirements. A survey of the radar manufacturing industry suggests that a solid-state transmitter will likely be a component of this radar. The ASR-11 will feature a digital weather processing channel to measure and display six calibrated levels of precipitation reflectivity. An additional weather surveillance goal is the capability to support detection of low altitude wind shear phenomena. Use of a low peak power, solid-state transmitter and associated pulse compression technology raises several issues with respect to the capability of ASR-11 to meet these weather measurement objectives:

1. ASR-11 sensitivity will be degraded by approximately 16 to 20 dB relative to the Klystron-based ASR-9 at short range. This results because it is not feasible to use pulse compression waveforms to compensate for low peak transmitted power at short range;

2. Stability of a solid state ASR-11 transmitter may significantly exceed that of previous vacuum tube ASR transmitters. Increased clutter suppression capability associated with this enhanced stability could partially offset the reduced sensitivity of ASR-11 in meeting weather detection goals;

3. Pulse compression range sidelobes may result in "ghost" images of actual weather features, displaced in range by as much as 10 km. In some circumstances, these could result in false indications of operationally significant weather features such as thunderstorm induced gust fronts.

We examine these issues through straightforward analyses and simulation. Our assessment depends heavily on Doppler weather radar measurements of thunderstorms and associated wind shear phenomena obtained with Lincoln Laboratory's Terminal Doppler Weather Radar and ASR-9 testbeds. Overall, our assessment indicates that a solid-state transmitter ASR-11 can provide six-level weather reflectivity data with accuracy comparable to that of the ASR-9. Detection of low altitude wind shear phenomena using a solid-state transmitter ASR is more problematic. Reduced sensitivity at short range–the range interval of primary operational concern for an on-airport ASR–results in significant degradation of its capability to measure the reflectivity and Doppler velocity signatures associated with gust fronts and "dry" microbursts. This degradation is not offset by the enhanced clutter suppression capability provided by a solid-state transmitter. Although pulse compression range sidelobes do not appear to be a major issue if they are held to the -55 dB level, simulations are presented where range sidelobes result in a false gust front wind shear signature.

ACKNOWLEDGMENTS

Our thanks to Paul Biron and Mark Isaminger who generated the microburst reflectivity distributions for Denver, Kansas City and Orlando that are shown in Figure 4 and used in the calculations leading to Tables 2, 3 and 4. Joe Cullen assisted us in identification of data sets for the simulations presented in Section 6.

TABLE OF CONTENTS

LIST OF ILLUSTRATIONS

LIST OF ILLUSTRATIONS
(Continued)

LIST OF TABLES

1. INTRODUCTION

In order to meet Advanced Automation System (AAS) requirements for digital terminal radars, the Federal Aviation Administration (FAA) has initiated a replacement program for aging Airport Surveillance Radars such as ASR-7 and ASR-8. This may lead to contract award for over 100 terminal area ASR-11s in 1996. A survey of the radar manufacturing industry suggests that a solid-state transmitter will likely be a component of this radar. In previous ASRs built using vacuum-tube based transmitters, necessary system availability has been assured by providing dual, redundant transmitting chains. Modern solid state transmitters use multiple, parallel power amplifier modules so that net output power need not drop below the required level when one or two modules fail. Since failed modules can be replaced while the transmitter continues to provide operational service, the necessity for a backup transmitting channel is removed. Life cycle operating and maintenance costs of a solid state transmitter are anticipated to be significantly lower than those of a tube-based system.

ASR-11 requirements include a digital weather processing channel that will measure and display six calibrated levels of precipitation reflectivity. A secondary goal is the capability to support detection of wind shear caused by thunderstorm-generated microbursts and gust fronts. This would be accomplished by interfacing the ASR-11 to the Wind Shear Processor (WSP) that has been developed for the ASR-9 [1]. Several major issues arise, however, in utilizing a solid-state transmitter ASR for weather surveillance:

1. A solid state ASR-11's sensitivity at short range will be 16 to 20 dB less than that of the Klystron-based ASR-9. This results because it is not possible to use pulse compression waveforms at short range to compensate for low peak transmitted power;

2. Stability of a solid state ASR-11 transmitter may significantly exceed that of previous ASRs. Increased clutter suppression capability associated with this enhanced stability could partially offset reduced sensitivity at short range. Ground clutter residue can be as important a factor as system noise in limiting radar detection of low cross-section weather phenomena;

3. Range sidelobes associated with the use of pulse-compression technology could smear weather echoes or produce false images of strong weather features.

In subsequent sections of this report, we examine these issues through straightforward analyses and simulation. While the study focuses on the ASR-11, results on pulse compression range sidelobes are relevant to the Terminal Area Surveillance System (TASS) program–a longer term research and development effort that is examining the use of radars with solid state transmitter and phased array antennae to perform rapid update, volumetric air traffic and weather surveillance. Section 2 delineates parameters of the radars that are candidates for the ASR-11 acquisition. In Section 3, we discuss the reduction in sensitivity at short range incurred through the use of a peak-power limited solid state transmitter. Section 4 addresses the extent to which improved clutter suppression would offset this sensitivity reduction. A simple discussion of range-sidelobe effects is presented in Section 5. In Section 6, a simulation of solid state ASR-11 measurements in a variety of weather and clutter scenarios illustrates, for specific cases, the degree to which a solid state radar's range sidelobes, reduced sensitivity and improved clutter-suppression capability would affect its weather sensing performance.

2. ASR-11 OVERVIEW

The ASR-11 is intended to replace aging ASR-7s and ASR-8s at FAA and military facilities that have not been equipped with the FAA's newest airport surveillance radar, the ASR-9. While the requirements and goals for the ASR-11 system are not finalized, in general the expectation is that this radar will provide the functional capabilities of the ASR-9. The ASR-11 is required to measure and display six calibrated levels of weather reflectivity, corresponding to the National Weather Service (NWS) standard levels illustrated in Table 1. A secondary weather surveillance "goal" is the capability to provide power-aperture product, ground clutter suppression and receiver dynamic range sufficient to support reliable operation of the WSP modification developed for the ASR-9.

Table 1.
National Weather Service Standard Weather Intensity Levels.

Weather Level	Reflectivity Interval	Precipitation Rate
1	18-30 dBZ	Light (Mist)
2	31-40 dBZ	Moderate
3	41-45 dBZ	Heavy
4	46-49 dBZ	Very Heavy
5	50-57 dBZ	Intense
6	> 57 dBZ	Extreme

The FAA's acquisition strategy for the ASR-11 is a "non-developmental item" (NDI) approach. An operational requirements document (ORD) and derived functional specification will be released to industry who will compete for award to build the ASR-11 based on existing "off-the-shelf" radar systems. These will obviously require some modification to interface with FAA National Airspace System (NAS) components such as the Remote Maintenance Monitoring System (RMMS) and AAS.

Seven NDI radars systems have been surveyed, five of which utilize solid state transmitters and pulse-compression waveforms. To achieve the necessary aircraft surveillance envelope, the solid state systems transmit peak powers of 10 to 25 KW, in combination with uncompressed pulse lengths varying from 50 to 100 μsec. These are in general non-linear FM waveforms which are compressed in the receiving chain to 1 μsec. For the radars surveyed, claimed peak range sidelobes vary from -40 to -55 dB (relative to the main lobe) for targets moving at Doppler velocities in the interval of concern for weather detection (+/- 50 m/sec). All candidate radars utilize a short, 1 μsec pulse at a different transmitted frequency to provide coverage at short ranges (i.e., ranges less than approximately half the long-pulse duration multiplied by the speed of light). Some of the systems exploit frequency diversity and/or pulse repetition interval (PRI) staggering schemes that vary somewhat from that of the ASR-9.

Other than the above, the surveyed radars employ parameters approximating those of the ASR-9. By requirement, they will operate in the 2.7-2.9 GHz band. Dual "high" and "low" antenna elevation patterns are cosecant-squared, with approximately 5° half-power elevation beamwidth and 1.5° azimuth beamwidth; the corresponding gains are about 34 dB. The reflectors are scanned in azimuth at a rate of approximately 12 rpm to provide update rates necessary for the aircraft tracker.

For specificity, in the remainder of this report we treat a radar with parameters approximating those of the ASR-9 when interfaced to a solid-state transmitter/receiver system recently tested at the FAA Technical Center (FAATC) [2]. That transmitter provided a 1 μsec, 22.5 KW uncoded pulse for detection out to 12 km and a 75 μsec, 22.5 KW coded pulse for detection beyond 12 km. The long pulse is compressed in the receiver to 1 μsec; measured range-sidelobe structure [2] is shown in Figure 1. As verified during testing of the system, this structure is largely invariant with target Doppler over the interval of concern for weather surveillance. We shall refer to this system as "ASR-SS". Note that our choice of specific parameters is for purposes of discussion only and does not imply that the ASR-11 will conform to these values.

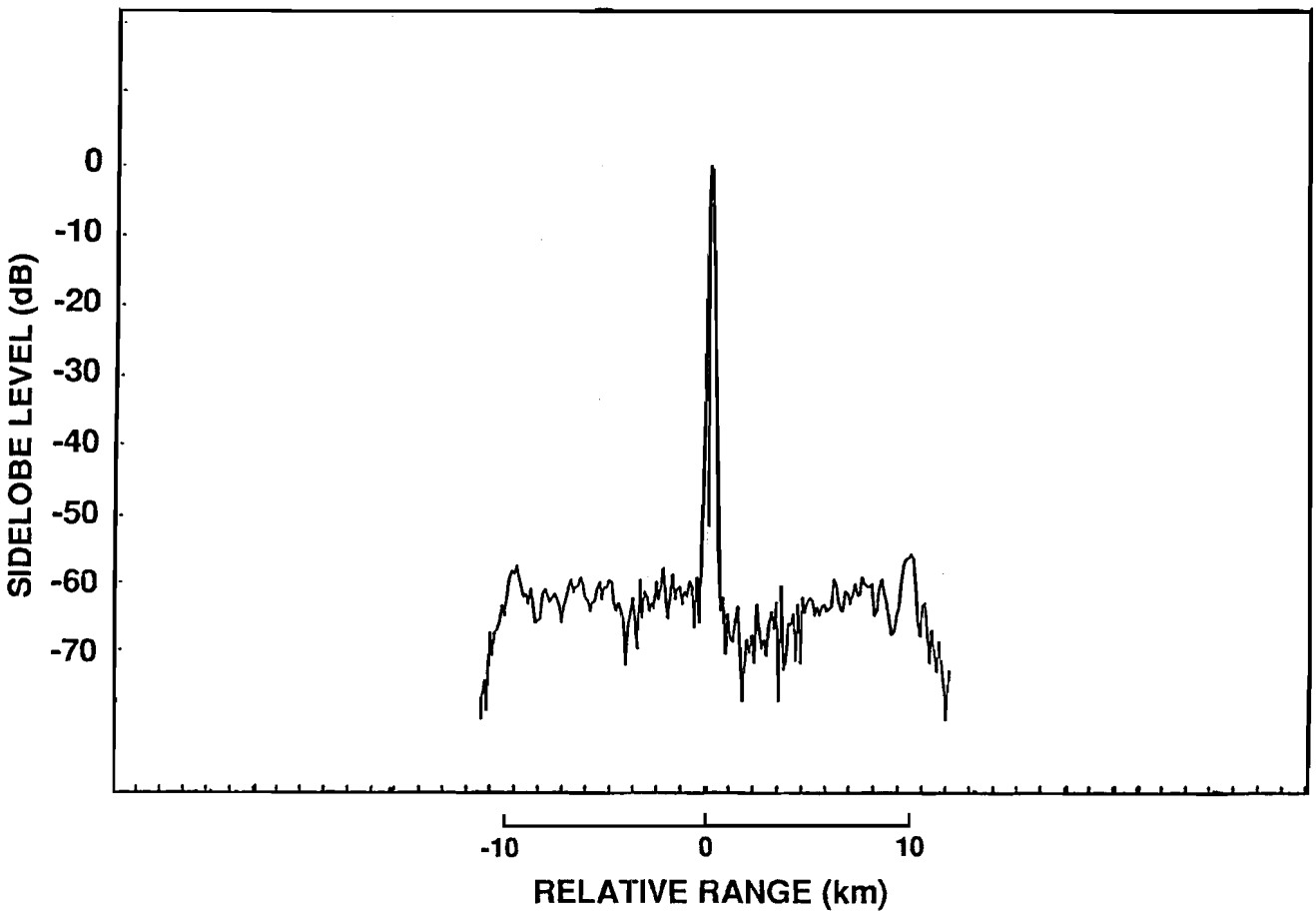

Figure 1. Range sidelobe structure (0 m/s target) of the solid state transmitter/receiver system interfaced to an ASR-9 for recent testing at the FAA Technical Center.

3. RADAR SENSITIVITY

In meteorological units, the system noise level for the ASR-SS using the solid-state transmitter would be equivalent to beamfilling weather of reflectivity:

$$10log(Z_N(R)) = 20\log\left(\frac{R}{R_o}\right) dBz \tag{1}$$

where R_o, the range at which this noise level equals 0 dBZ, is

$$R_o = 3.4km \quad \text{(short pulse)} \tag{2}$$

$$= 29.8km \quad \text{(long pulse)}$$

These equations assume that the radar receiving chain is configured such that sensitivity time control (STC) or automatic gain control (AGC) circuits do not introduce an additional decrease in the signal-to-noise ratio (SNR). The composite sensitivity assuming a switch from short to long pulse at 12 km range is shown in Figure 2. For comparison, the ASR-9 with its 1 MW, 1 μsec uncoded pulsed is 16 dB more sensitive than the curve indicated in Figure 2 at ranges less than 12 km, and 2 dB less sensitive outside that range.

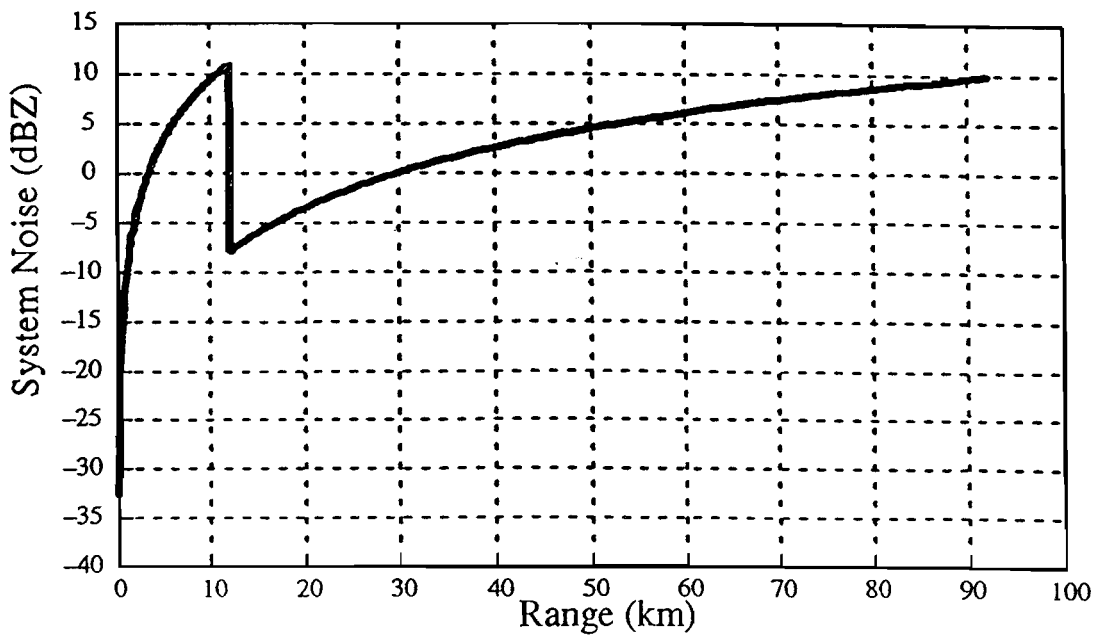

Figure 2. System noise level of ASR-SS expressed in units of equivalent precipitation reflectivity factor (dBZ). The discontinuity at 12 km coincides with the switch from use of the 1 μsec uncompressed pulse to the 75 μsec pulse compression waveform.

The indicated sensitivity for ASR-SS is adequate for six-level precipitation reflectivity measurement, providing at least 7 dB SNR for weather at the level one threshold. Detection of wind shear phenomena in the short-range interval where the uncompressed pulse would be used is more problematic. In addition to the low intrinsic reflectivity of some forms of wind shear ("dry" microbursts and gust fronts), the thunderstorm outflows that generate low altitude wind shear extend only a few hundred meters into the atmosphere and therefore produce significant "beamfilling loss" when illuminated by an ASR's fan-shaped elevation beam. Depending on range to the event, depth of the outflow and whether the ASR's high- or low-elevation receiving beam is used, the beamfilling loss can vary from 0 to 15 dB [3]. Figure 3 plots the beamfilling loss for an ASR-9 as a function of range, assuming various outflow depths. The curves are appropriate for this study since all the candidate ASR-11 NDI radars have antenna elevation patterns very similar to that of the ASR-9.

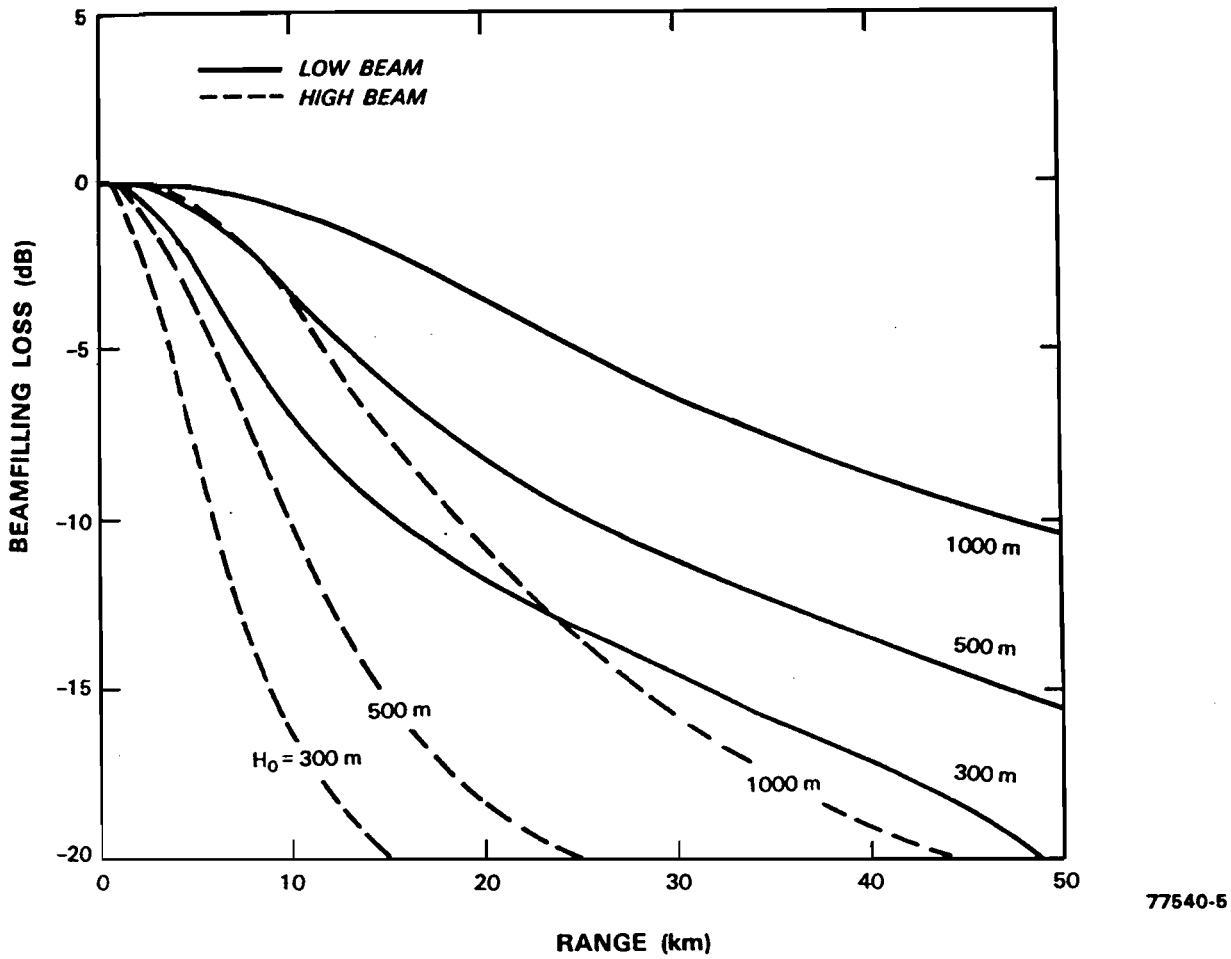

Figure 3. Beamfilling loss as a function of range for a low altitude thunderstorm outflow measured with an ASR. Solid and dashed curves correspond to use of the low and high receiving beams. Curves are calculated assuming outflow depths (H_0) that vary from 300 m to 1000 m. From [3].

In interpreting Figure 2 relative to the capability of ASR-SS to measure microburst wind shear, we will assume:

1. A 6 dB SNR requirement for accurate velocity estimation;

2. Beamfilling loss that corresponds to a 500 m deep outflow. At 12 km, the range of minimum sensitivity for ASR-SS, the beamfilling loss is 12 dB for the high beam. Microburst detection with an ASR requires adequate SNR in both high and low receiving beams [4].

With the above assumptions, Figure 2 implies that ASR-SS will require 29 dBZ or greater reflectivity in order to measure the wind pattern associated with microbursts at its range of minimum sensitivity.

Figures 4a and 4b show distributions of microburst outflow reflectivities in "wet" (Orlando, FL), "dry" (Denver, CO) and intermediate (Kansas City, KS) environments. These were generated using data from Lincoln Laboratory's Terminal Doppler Weather Radar (TDWR) testbed which has operated for at least one year at each of these sites. Figure 4a treats the maximum (in time and space) surface reflectivity for the microbursts; Figure 4b gives the distribution for reflectivities in the outflow velocity cores of the microbursts–the highest radial wind areas of the approaching and receding outflow which have often moved away from the higher reflectivity rain shaft that generates the microburst.

While most microbursts in the Orlando and Kansas City environments exhibit maximum reflectivities well above the system noise equivalent reflectivity of ASR-SS, the substantially lower reflectivity values in the outflow velocity cores may approach that noise level. In Denver, only 45 percent of microbursts in the data set exhibited even peak reflectivities exceeding the above 29 dBZ requirement for detection at the range of minimum sensitivity; a minority 15 percent of the outflow velocity cores were associated with this reflectivity or greater. In instances where a microburst's maximum reflectivity exceeds ASR-SS's SNR requirement, but the outflow velocity core reflectivity does not, the microburst might not be detected at all; alternately, it might be detected but with a downwards bias in the estimate of its size and intensity.

Gust front detection with airport surveillance radars requires measurement and recognition of the "thin-line" echo that often delineates the leading edge of the front. This signature is recognizable as a moving line of enhanced reflectivity and/or spatially coherent Doppler velocity embedded in a background of noise. Robust detection of gust front thin lines with a "Machine Intelligent" gust front detection algorithm (MIGFA) [5] has demonstrated that detection of these features at SNRs approaching 0 dB is feasible. For discussion purposes, we will argue that:

1. Beamfilling loss corresponds to a typical 1000 m gust front depth and use of the low receiving beam. (Gust front thin line measurement with the ASR-WSP does not require use of the high receiving beam). Beamfilling loss at 12 km range, for example, is therefore 2 dB;

2. A 3 dB SNR is required for adequate measurement of the reflectivity and/or Doppler velocity thin-line signature. Note that this differs from the requirement cited previously with respect to microburst detection. Here, the velocity measurement serves only as a means of detecting the slightly enhanced signal strength associated with the thin-line echo. Accurate estimation of the velocity values is not required.

With these assumptions, a gust front thin line's reflectivity must exceed 16 dBZ to be detected by ASR-SS at its range of minimum sensitivity.

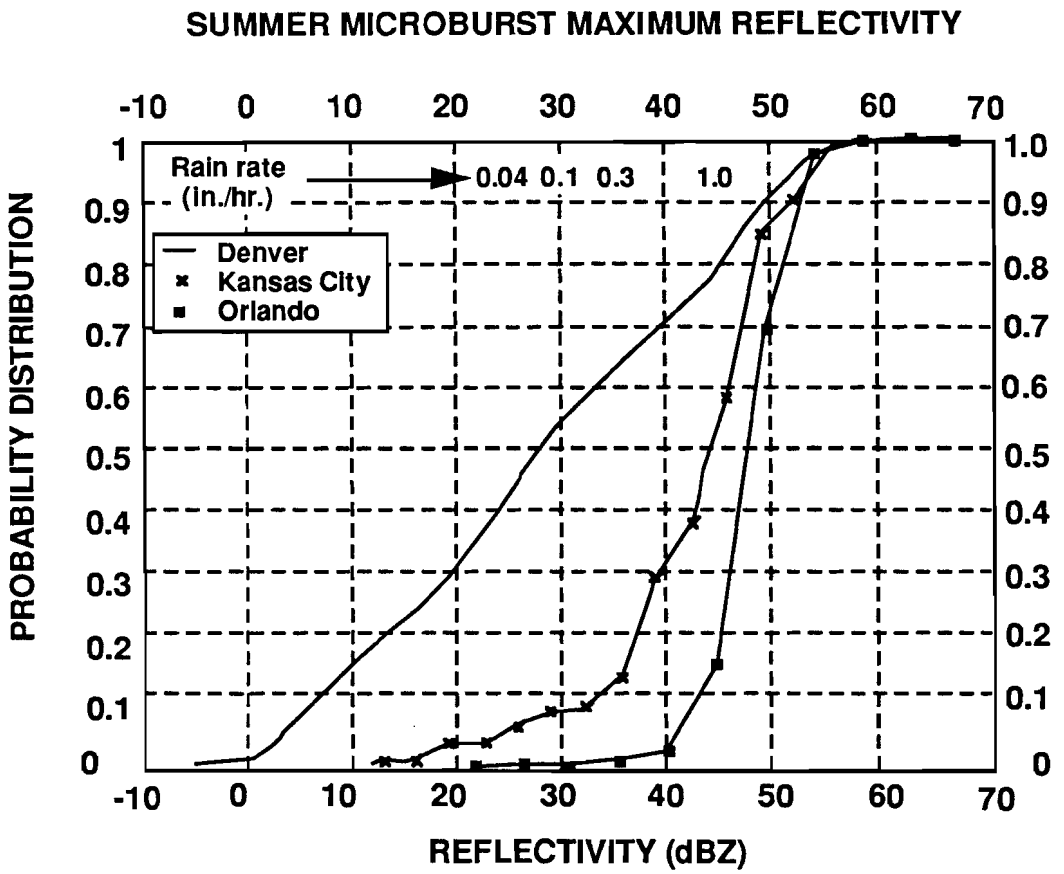

Figure 4a. Cumulative distributions of microburst maximum reflectivity factor for Orlando, Kansas City and Denver. Distributions are compiled from data collected with Lincoln Laboratory's TDWR testbed over at least one year of operations at each site.

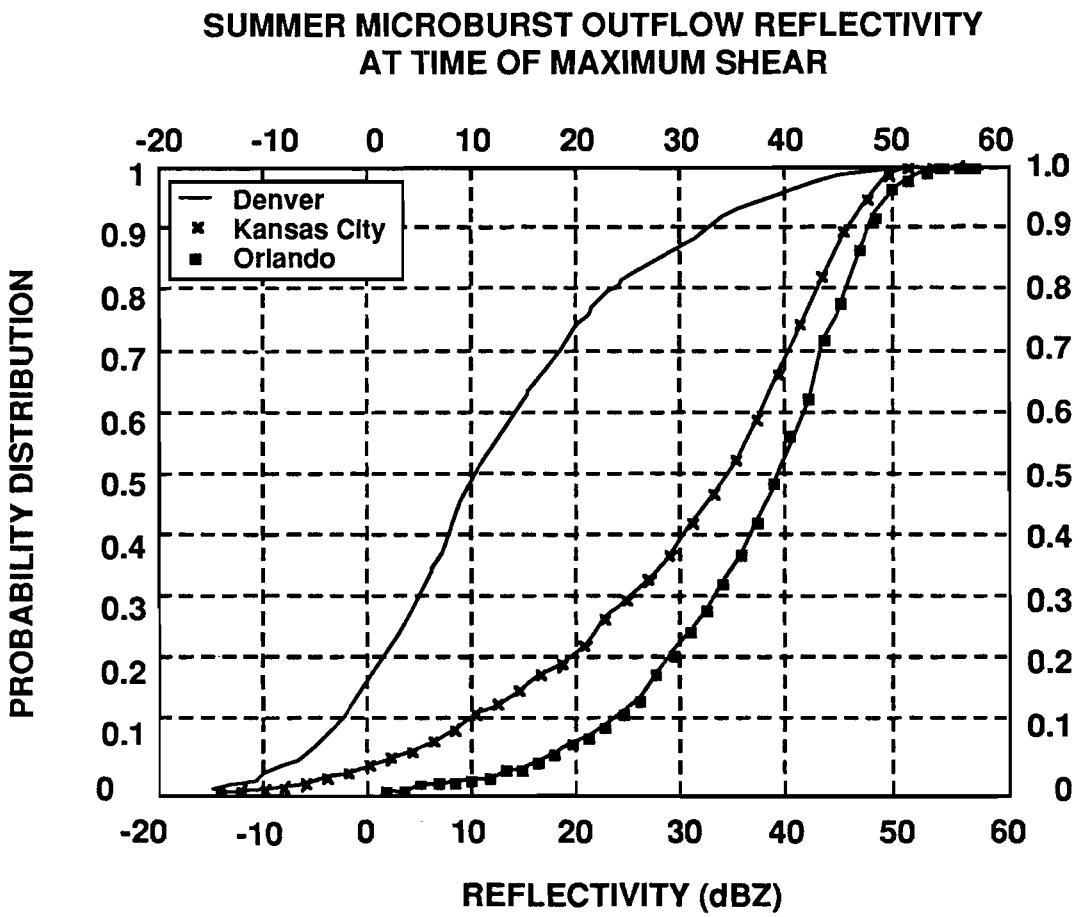

Figure 4b. Cumulative distributions of reflectivity factor for the points of maximum approaching and receding radial velocity in Orlando, Kansas City and Denver microbursts. This "outflow velocity core" is often displaced from the higher reflectivity rain shaft that generates the outflow.

Histograms of gust front thin line reflectivity (averaged along the length of the front) are shown for Denver, Kansas City and Orlando in Figure 5 (from reference [6]). Overall, only about 5 percent of the gust fronts tabulated exhibited reflectivities in excess of the 16 dBZ threshold for ASR-SS at its range of minimum sensitivity. While MIGFA's ability to "coast" a gust front across the annulus of reduced sensitivity might enable detection of some fronts with lower average reflectivity, ASR-SS would clearly perform significantly poorer than the ASR-9, whose transmitter provides adequate peak power for detection of the majority of these fronts. The data in Figure 5 do not show clear site-to-site differences for the distributions of gust thin-line reflectivities. We have noted, however, that thin-line reflectivities at our ASR-9 test site in Albuquerque, NM are significantly lower than those tabulated in Figure 5. Maximum thin line reflectivities at Albuquerque are 5 to 10 dBZ, with events in the -20 to 0 dBZ interval common. Detection of gust fronts in this environment is difficult with the ASR-9 and would be virtually impossible for ASR-SS.

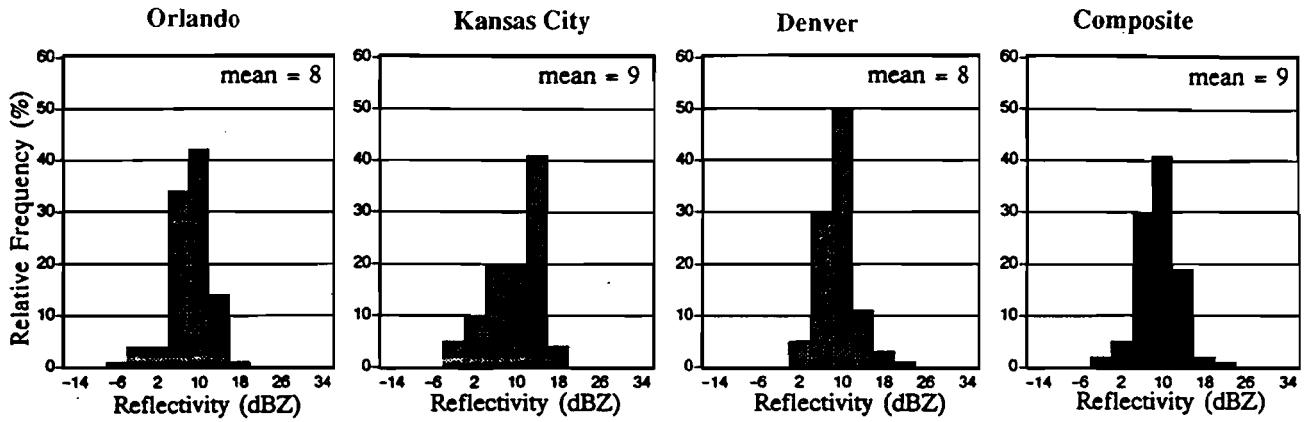

Figure 5. Histograms of reflectivity factor in gust front thin lines (averaged along the length of the front). Data are from TDWR testbed operations at Orlando, Kansas City and Denver. The fourth plot is the composite distribution for the three sites. From [6].

The microburst and gust front reflectivity distributions presented above can be used to calculate a range-averaged measure of the fraction of wind shear events that would exceed the SNR requirement of ASR-SS. This fraction is given by:

$$F_{SNR} = \frac{1}{R_{\max}} \int_0^{R_{max}} \int_{Z_N(R)+BL(R)+T_W}^{\infty} p(Z_W)\, dZ_W\, dR \qquad (3)$$

Here $R_{\max}$, the maximum range of operational concern for wind shear detection, is taken to be 15 km. $Z_N(R)$ is the system noise level equivalent reflectivity defined in equations (1) and (2), $BL(R)$ is the beamfilling loss and T_W is the SNR requirement for accurate velocity measurement. Finally, $p(Z_W)$ is the probability density function of reflectivity for the various environment/wind shear type categories, derived from Figures 4 and 5. Table 2 compares representative values of this fractional visibility for ASR-SS and ASR-9 using the Orlando and Denver "outflow" reflectivity distributions and the site-averaged gust front thin line distribution. For these distributions, ASR-SS's reduced sensitivity results in a nine to 34 percent lowering–relative to ASR-9–of the fraction of wind shear events where adequate SNR would be achieved.

Table 2.
Range-Averaged Fractional Visibility of Wind Shear Events as Defined by Equation (3)

	Denver Outflow	Orlando Outflow	Gust Front
ASR-SS	0.30	0.87	0.64
ASR-9	0.56	0.96	0.98

4. GROUND CLUTTER

The discussion in Section 3 clearly indicates that, from an SNR perspective, utilization of the solid state transmitter is appropriate for six-level weather detection but would result in significant degradation in the reliability of ASR-based microburst or gust front detection, particularly at High Plains airports where "dry" microburst or gust front activity is frequent. Partially offsetting this would be improved ground clutter suppression capability resulting from ASR-SS's more stable transmit chain. Ground clutter residue limits the capability of an ASR to detect low altitude wind shear when the associated reflectivity is approximately 20 dBZ or less [7]. An important factor here is the impact of transmitter instability residue which, in the case of the ASR-9, limits achievable clutter suppression to about 48 dB.

Measured instability residue for ASR-SS was 62 dB [2]. Most of the solid-state transmitter systems proposed for ASR-11 feature claimed transmitter instability residues in the range of 60 to 65 dB. While it is doubtful that–at this level–transmitter instability will be the limiting factor in clutter suppression capability (intrinsic non-zero Doppler components in the clutter spectrum and the effects of antenna scanning will probably be more important) we will assume the most favorable case where ASR-SS achieves the full 62 dB of clutter suppression.

Figure 6 shows a histogram of the gate-by-gate ground clutter intensities measured by Lincoln Laboratory's ASR-9 testbed in a moderate (Orlando, FL) clutter environment; a corresponding histogram for a severe environment (Albuquerque, NM) appears in Figure 7. The clutter returns are from the low receiving beam and have been scaled to an equivalent weather reflectivity factor. The histograms treat the range interval from 0 to 15 km. Median and 90th percentile clutter intensities are 25 and 50 dBZ for Orlando and 32 and 60 dBZ for Albuquerque.

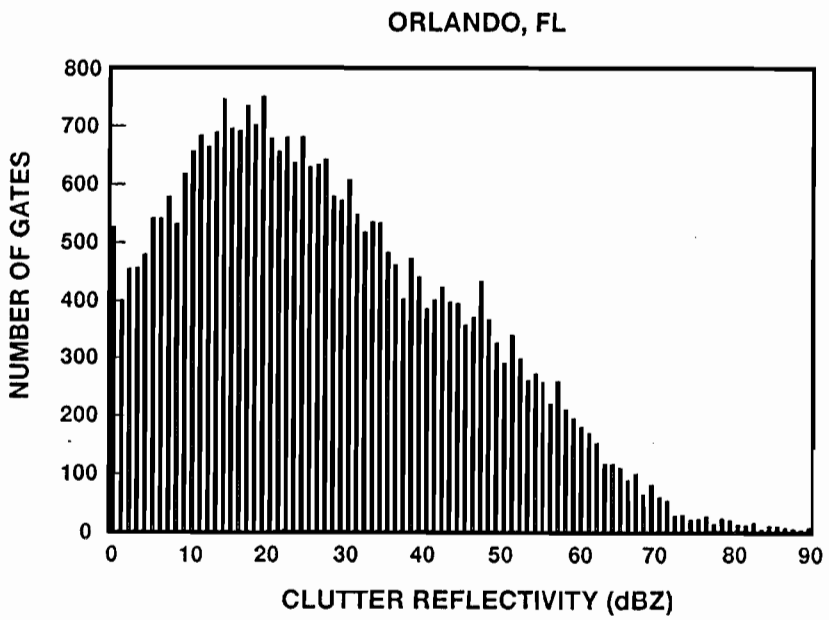

Figure 6. Histogram of low beam ground clutter equivalent reflectivity factor measured with Lincoln Laboratory's ASR-9 testbed at Orlando. Histogram treats range interval (0 to 15 km) of primary operational concern for low altitude wind shear detection.

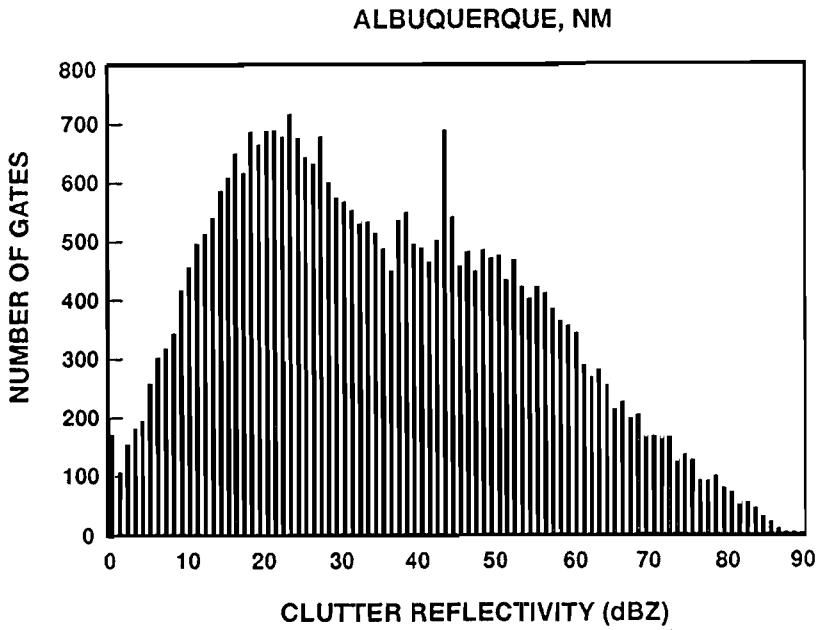

Figure 7. Histogram of low beam ground clutter equivalent reflectivity factor measured with ASR-9 testbed at Albuquerque. Histogram treats range interval from 0 to 15 km.

As was the case with the sensitivity issue, both the Klystron ASR-9 and ASR-SS provide clutter suppression adequate for measurement of six-level weather reflectivity. We assume, as in [7], that accurate reflectivity measurement with an ASR requires an approximately 10 dB weather-to-clutter-residue power ratio and that attenuations of 48 and 62 dB are achievable with the respective radars. Figures 6 and 7 then imply that, for ASR-SS, weather at the level one threshold reflectivity will be obscured by ground clutter residue in one percent of resolution cells in the Orlando clutter environment, and four percent of resolution cells at Albuquerque. Corresponding percentages for ASR-9 are 10 percent and 19 percent. These percentages are acceptable given that the ASR-11's weather processor will use spatial operators to fill in weather values for many clutter-obscured resolution cells. Level 2 weather returns–which correspond to rain rates at which precipitation begins to have significant operational impact–would be subject to negligible clutter obscuration.

The lower reflectivities that may be associated with microburst and gust front phenomena make clutter suppression limitations more relevant to low altitude wind shear detection. The microburst and gust front reflectivity distributions presented in Section 3 can be combined with Figure 6 or 7 to derive a measure of the clutter-residue obscuration for the various environment/wind-shear type combinations. If $p(Z_C)$ is the density function corresponding to the clutter intensity distribution shown in the figures, and $p(Z_W)$ is the appropriate wind shear

event reflectivity distribution as before, then the areally averaged fraction of wind shear events that is not obscured by clutter residue is:

$$F_C = \int_0^{\infty} p(Z_C) \int_{Z_c - S + T_c}^{\infty} p(Z_W)\, dZ_C\, dZ_W \qquad (4)$$

Here S is the clutter suppression capability of the radar and T_C is the required weather-to-clutter-residue power ratio, again taken as 10 dB. ($S - T_C$ corresponds to the "subclutter visibility" metric commonly used in radar system definition.) This fraction cannot be equated to a wind shear event detection probability since the spatial distribution of the obscured cells is important in determining the latter. However, it provides a useful means for comparing the relative impact of clutter residue for an ASR-9 and the more stable ASR-SS. Table 3 lists this fractional wind shear event visibility for the two radars assuming both Albuquerque and Orlando ground clutter environments and the wind shear reflectivity distributions used in Table 2. A range-averaged beamfilling loss correction has been applied to the weather reflectivity distributions prior to evaluation of Equation (4).

Table 3.
Fractional Visibility of Wind Shear Events in the Presence of Ground Clutter Residue as Defined by Equation (4).

	ABQ Clutter			ORL Clutter		
	Denver Outflow	Orlando Outflow	Gust Front	Denver Outflow	Orlando Outflow	Gust Front
ASR-SS	0.85	0.99	0.90	0.92	1.0	0.95
ASR-9	0.68	0.94	0.72	0.79	0.97	0.84

Table 3 confirms that, relative to the ASR-9, the improved stability of a solid-state transmitter radar should reduce obscuration of "dry" wind shear phenomena by ground clutter residue, particularly in a severe clutter environment such as Albuquerque. To ascertain the degree to which this offsets the associated loss of sensitivity, we combine the fractional visibilities defined by Equations (3) and (4) to estimate the areally averaged fraction of wind shear events that are obscured by neither ground clutter residue nor system noise. If we assume that the two interference sources are independent, the corresponding values in Tables 2 and 3 can simply be multiplied to obtain the composite fractional visibilities shown in Table 4. In fact, obscuration by clutter residue is most likely at short range where on average, clutter is strongest, while system noise (scaled to weather reflectivity units) increases with increasing range and is therefore most likely to cause obscuration at longer range. Accounting for this relation would decrease the values in Table 4 but would not significantly change the important result, the relative visibilities for ASR-9 and ASR-SS.

Table 4.
Fractional Visibility of Wind Shear Events in the Presence of Both Ground Clutter Residue and Noise.

	ABQ Clutter			ORL Clutter		
	Denver Outflow	Orlando Outflow	Gust Front	Denver Outflow	Orlando Outflow	Gust Front
ASR-SS	0.26	0.86	0.58	0.28	0.87	0.61
ASR-9	0.38	0.90	0.71	0.44	0.93	0.82

The numbers indicate that, on a relative basis, a solid state transmitter ASR would overall have less capability for the detection of wind shear phenomena than an ASR-9, even in a severe ground clutter environment where its increased stability should yield the greatest benefit. The differential "fractional visibility" for the two systems varies from as little as 4 percent to as much as 21 percent depending on the clutter environment and wind shear category considered. We reiterate that these values do not equate to detection probabilities: they do not account for resolution cell-to-cell correlation of the interferers which is an important factor for the detectability of a distributed weather target, they do not consider other sources of interference such as echoes from precipitation above the low altitude wind shear layer, and a number of simplifying assumptions have been made.

5. PULSE COMPRESSION RANGE SIDELOBES

In the Appendix to this report we show that the effects of pulse-compression range sidelobes on weather images can be simulated by convolving the range sidelobe function with the actual range distribution of weather reflectivity and radial velocity. Three simple examples illustrate the major effects. Peak range sidelobes of -55 dB and -40 dB are assumed to encompass the interval quoted by vendors of the NDI radars surveyed for the ASR-11 acquisition; the modeled range-sidelobe structures are plotted in Figure A.1.

Figure 8 simulates a pulse-compression receiver's output when the range extent of a significant weather feature–2 km in this illustration–is small relative to the spatial extent of the uncompressed pulse. An example would be a narrow rain band or squall line oriented roughly perpendicular to the radar beam. When measured with the pulse-compression waveform, the output weather image roughly replicates in range the sidelobe structure of the waveform, *albeit* subject to "low-pass filtering" by the finite width weather feature. For squall lines with reflectivities exceeding 50 to 60 dBZ, these sidelobe effects could plausibly mimic gust front thin lines or other low reflectivity weather features preceding or trailing the storm.

A second case is treated in Figure 9 where the weather feature is taken to have a sharp leading edge but extends over a range interval that is comparable to the extent of the uncompressed pulse. Multicellular thunderstorms could exhibit such a reflectivity distribution. In this case, the integral of the portion of the sidelobe structure that overlaps the weather echo is the important parameter. The pulse compression waveform smears the storm's leading edge into the echo free area ahead of it; this "spillover's" intensity decreases monotonically with distance from the storm front. Operationally, the spillover would indicate precipitation in regions that are actually rain free and would decrease the apparent magnitude of the reflectivity gradient at the storm's leading edge. Sharp reflectivity gradients are often interpreted as being indicative of severe weather.

A final example (Figure 10) treats a distribution of reflectivity that is also extensive in range but exhibits a more gradual transition from the "clear air" reflectivity ahead of the storm. Decaying thunderstorms and non-convective precipitation systems may display weak, leading edge gradients. The considerations of the preceding example apply here; however, because the pulse-compression "spillover" is now superimposed on actual precipitation echoes, the artifact is masked.

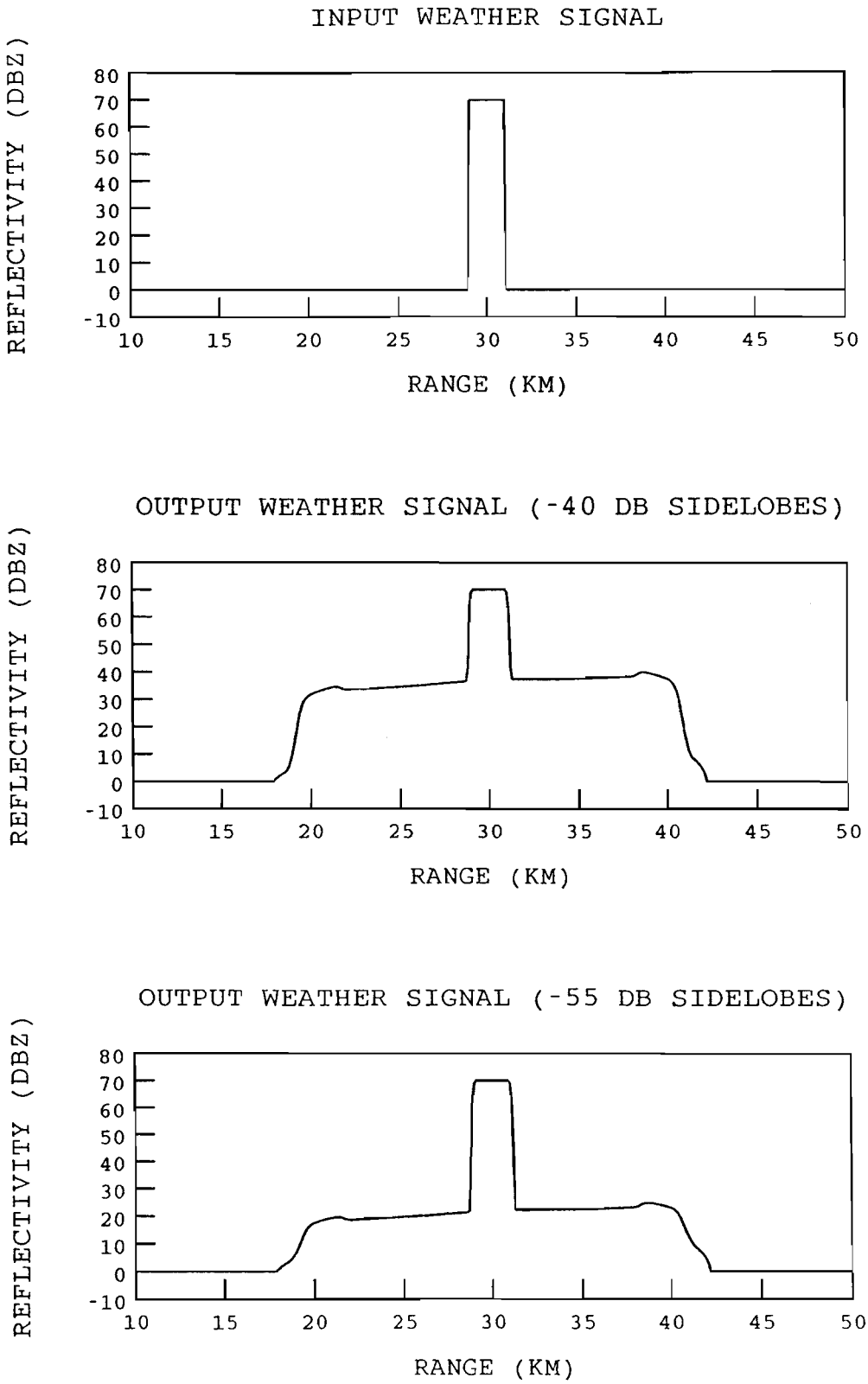

Figure 8. Simulations of the output of a pulse compression receiver for the indicated precipitation reflectivity distribution in range. Range sidelobe structures plotted in Figures A-1 are assumed.

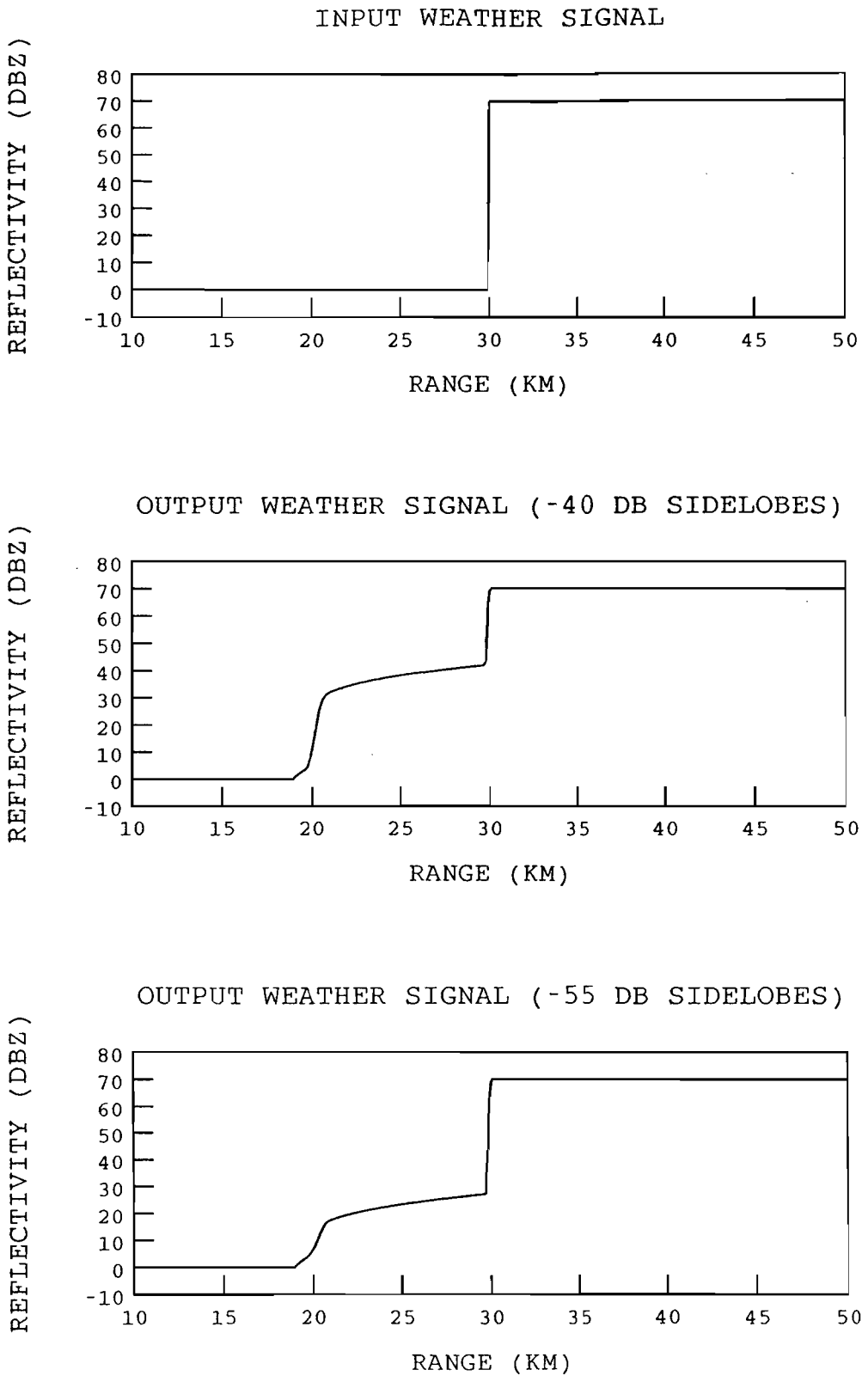

Figure 9. Simulations of the output of a pulse compression receiver for the indicated precipitation reflectivity distribution in range.

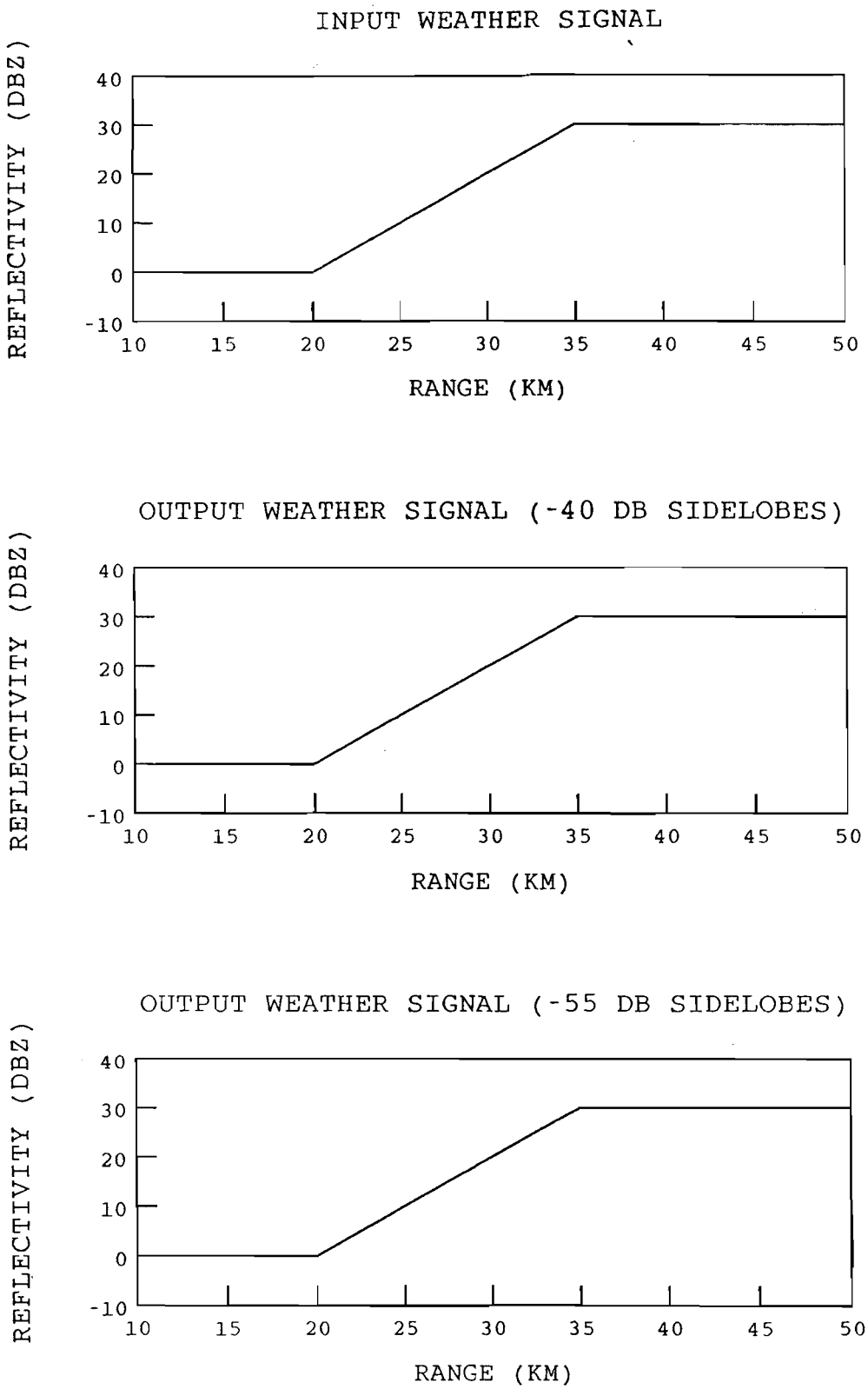

Figure 10. Simulations of the output of a pulse compression receiver for the indicated precipitation reflectivity distribution in range.

In summary, these simple examples illustrate the point made further through simulations with actual weather scenarios in Section 6: artifacts generated by pulse-compression range sidelobes will be most prominent in severe weather conditions where echo reflectivity is high and spatial gradients are large. In these conditions, scenarios can be envisaged that would result in operations-impacting false weather indications. The simulations in the next section examine the extent to which, in practice, such conditions actually occur.

6. SIMULATED WEATHER IMAGES FROM ASR-SS

The Appendix describes a procedure for simulating ASR-SS weather images utilizing data from short-pulse radars–in our case, Lincoln Laboratory's TDWR and ASR-9 testbeds or the University of North Dakota's (UND) Doppler weather radar. The weather images from these radars can be treated as "truth" in the sense that:

1. The sensitivity of the testbed radars is comparable to or exceeds that of ASR-SS;

2. The images we examine are free of significant clutter-residue contamination;

3. These short-pulse radars are not subject to effects from range sidelobes at distances displaced more than a few hundred meters from the primary pulse resolution volume.

Briefly, the simulation involves "range filtering" of weather reflectivity or radial velocity images from the short-pulse radars with kernels derived from the assumed range sidelobe structure. Ground clutter reflectivity images, measured with our ASR-9 testbed at Orlando and Albuquerque, are then superimposed after first reducing these by the clutter suppression capability assumed for ASR-SS. In the resultant images, the ratios of signal to noise and signal to clutter residue are calculated for each resolution cell and pixels are deleted from the image where these ratios do not exceed 5 and 10 dB, respectively.

We first examine the ground clutter images. Figure 11 shows the Orlando and Albuquerque measured clutter distributions from the ASR-9 testbed. Panels (a) and (c) are the equivalent precipitation reflectivity factor of low-beam ground clutter prior to high-pass filtering. Panels (b) and (d) are the output of 17-coefficient finite impulse response filters that provide maximum clutter suppression of approximately 48 dB. Clutter residue levels are as high as 35 dBZ at Orlando and 50 dBZ at Albuquerque. Corresponding clutter distributions for ASR-SS are simulated in Figure 12. Although spreading of the strong clutter returns caused by the pulse-compression range sidelobes is evident prior to clutter suppression (panels (a) and (c)), the assumed 62 dB suppression capability more than compensates. Maximum clutter residue levels are about 35 dBZ, even in Albuquerque's mountain clutter environment. We reiterate that this comparison assumes (probably unrealistically) that transmitter instability is the limiting factor in ASR-SS's capability to suppress ground clutter.

Figure 13 illustrates the simulation process for an Orlando weather scenario consisting of scattered airmass thunderstorms and two gust front thin lines. For purpose of illustration, we have raised the peak range sidelobes shown in Figure A-1 to -25 dB to emphasize their effect. The input weather map is shown in part (a). Convolution with the artificially high range sidelobes (panel b) results in substantial range-smearing and/or ghosting of the echoes at ranges beyond 12 km where ASR-SS uses pulse compression. Elimination of resolution cells with inadequate SNR (panel c) significantly reduces the observability of the gust front thin lines inside 12 km, particularly the weaker front northwest of the radar. Inclusion of clutter residue (from Albuquerque) (panel d) has little additional effect on the observability of the weather features.

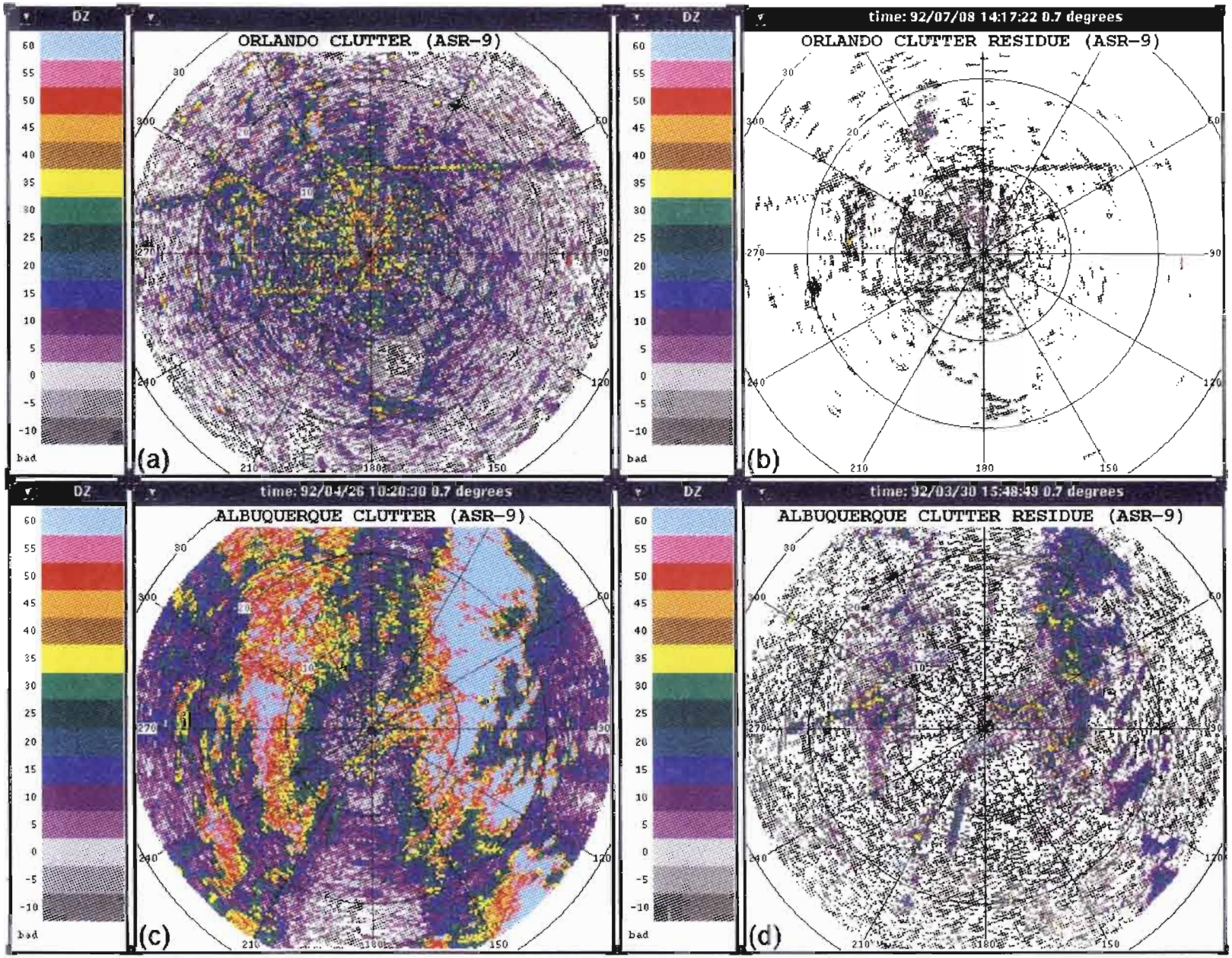

Figure 11. PPI displays of ground clutter equivalent precipitation reflectivity factor measured with ASR-9 testbed. Panels (a) and (c) show unfiltered clutter at Orlando and Albuquerque. Panels (b) and (d) are clutter residue at the output of high-pass clutter suppression filters used by the ASR-9 Wind Shear Processor.

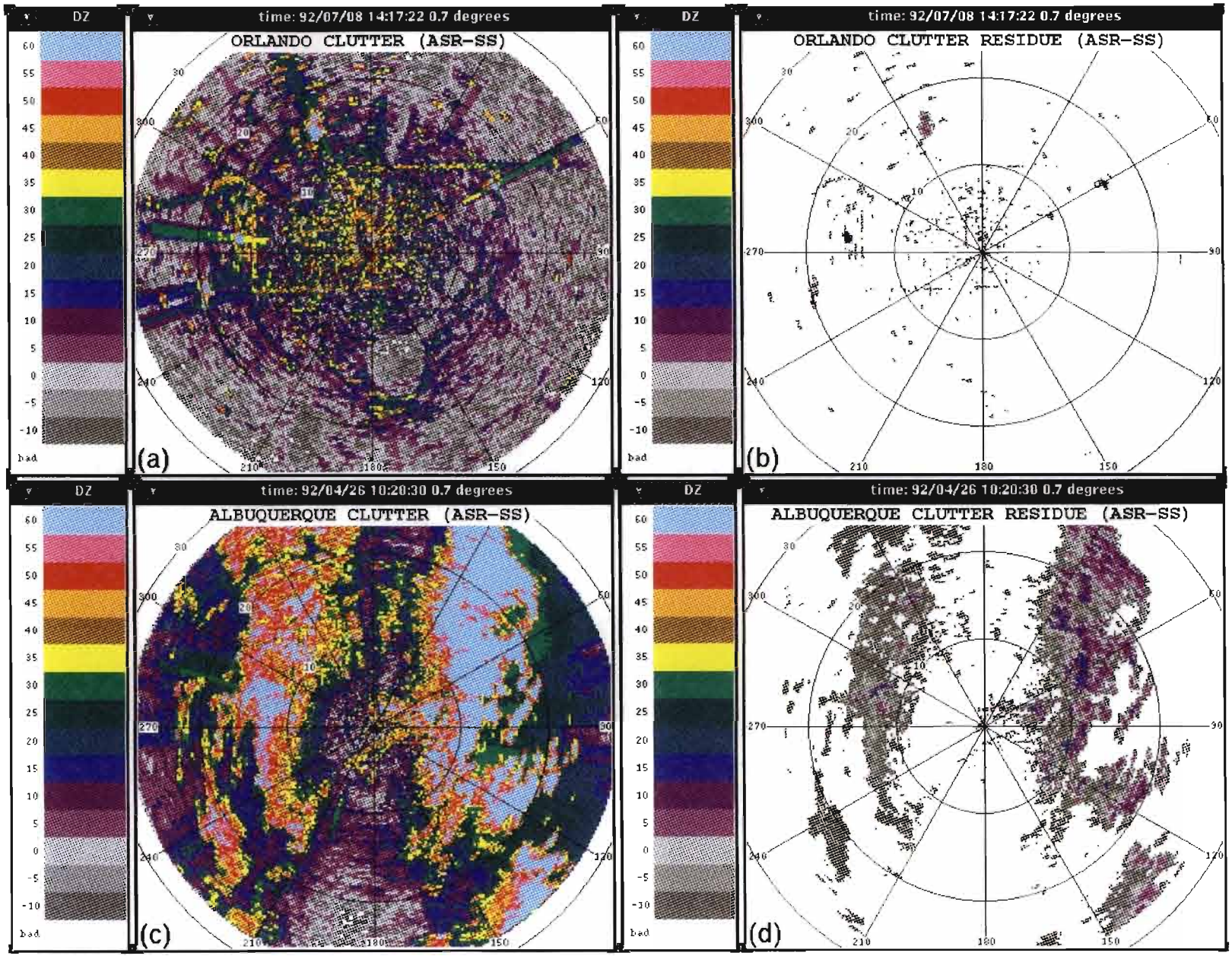

Figure 12. PPI displays of ground clutter equivalent precipitation reflectivity factor simulated for ASR-SS. Panels (a) and (c) simulate unfiltered output of pulse compression receiver for Orlando and Albuquerque, assuming the -55 dB peak range sidelobe structure shown in Figure A-1. Panels (b) and (d) are simulations of clutter residue for ASR-SS, assuming that the solid state transmitter supports 62 dB suppression of the ground clutter echoes.

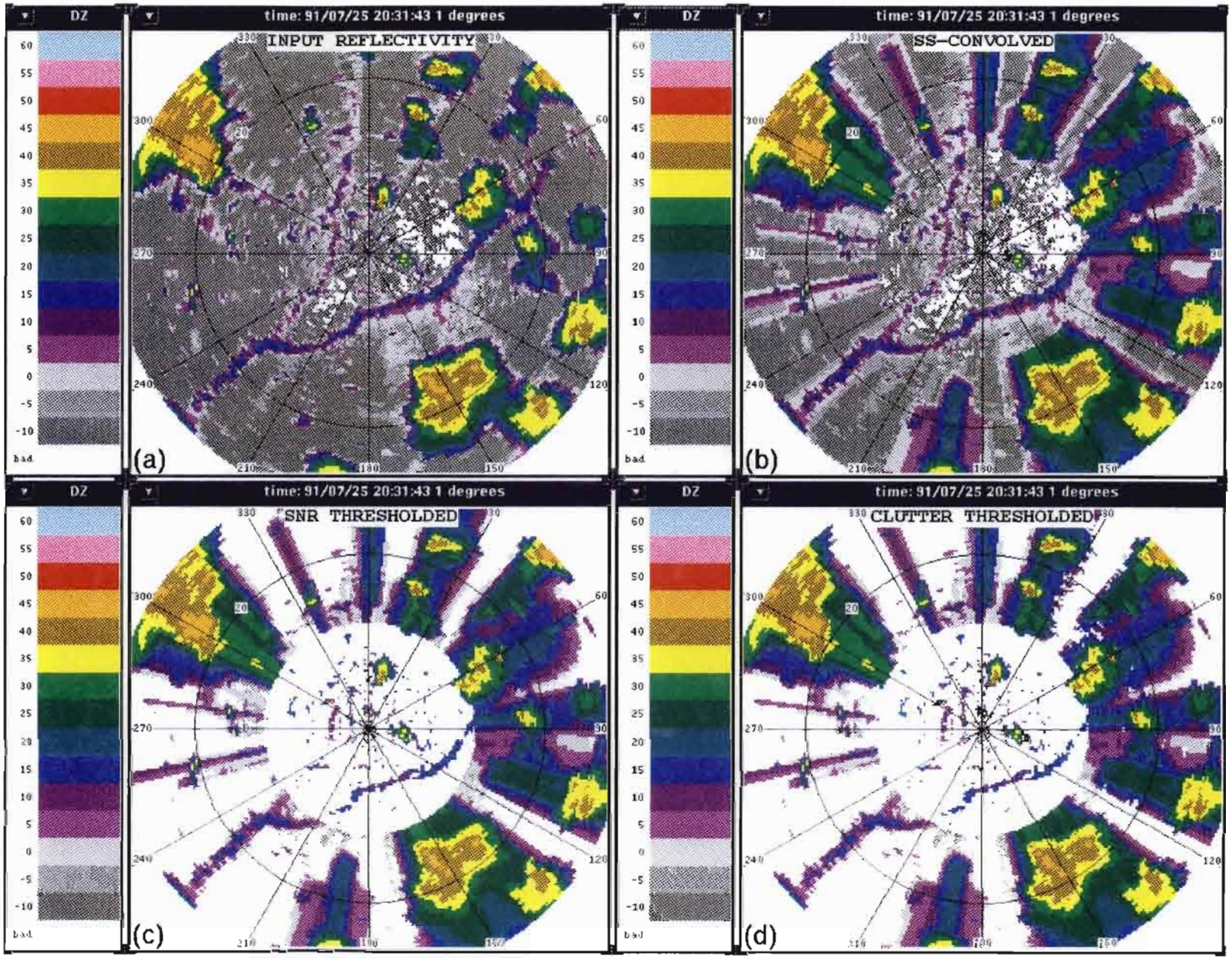

Figure 13. Illustration of simulation of weather reflectivity factor measurement with solid state transmitter ASR. Panel (a) is input reflectivity PPI from ASR-9 testbed. In panel (b), this image has been convolved with the range sidelobe structure of a pulse compression transmitter/receiver system as in Equation A-6. Range sidelobe structure is similar to Figures A-1 except that peak sidelobes are set artificially high (-25 dB) to make "ghosting" of weather echoes obvious. In panel (c), resolution cells where SNR does not exceed 5 dB are deleted from image. In panel (d), resolution cells where weather signal to clutter residue does not also exceed 10 dB are deleted from image. Simulation uses measured ground clutter from Lincoln Laboratory testbed in Albuquerque.

Figures 14-17 illustrate short-range sensitivity loss with ASR-SS. In Figure 14, two north-south oriented gust front thin lines can be seen east and west of the radar in the original TDWR image (panel (a)). Panel (b) simulates the sensitivity of the Klystron transmitter ASR-9. Although there is a loss of clear-air background measurement, the ASR-9 sensitivity is sufficient to measure the gust front thin lines with minimal signature degradation. By contrast, ASR-SS simulations (panels (c) and (d) assume, respectively, -55 and -40 dB peak range sidelobes) show almost complete loss of the western thin line signature and noticeable fragmentation of the thin line to the east. Note also the range-sidelobe induced ghosting for many of the thunderstorms in the image.

Figure 15 is another example of gust front thin line fragmentation at short range owing to the reduced sensitivity of ASR-SS. In this case, MIGFA could maintain track on the gust front approaching the radar only through the use of "anticipation" (based on previous longer range detection of the front) and extrapolation from the more observable portion of the front to the north of the radar.

"Dry" microburst measurements assuming the parameters of ASR-9 and ASR-SS are simulated in Figure 16. Input data are from the TDWR testbed operated in Denver. Locations of the microbursts are outlined in red. The ASR-9 has sufficient sensitivity to readily measure the velocity divergence signature associated with each of the three events (panels (a) and (b)). For ASR-SS, sensitivity is insufficient to measure the divergence at 9.5 km, 128° and results in significant degradation of the signature of the microburst at 12.5 km, 150°. The third microburst at 8 km, 230° has the highest reflectivity (25 dBZ) of the three events and its signature is largely unaffected by the sensitivity limits of ASR-SS.

A final gust front thin line example illustrates the tradeoff between reduced short-range sensitivity for ASR-SS and its increased clutter suppression capability. In Figure 17, we simulate ASR-9 (panels (a) and (b)) and ASR-SS (panels (c) and (d)) measurements of a thin line echo. The left-hand panels superimpose clutter residue from the moderate Orlando clutter environment and the right-hand panels superimpose severe Albuquerque clutter residue. For ASR-9, sensitivity is adequate to measure the entire length of the thin line, but clutter residue in the Albuquerque environment would totally obscure the northeastern portion of the signature. Conversely, for ASR-SS radar sensitivity significantly degrades measurement of a portion of the front inside 12 km, but its improved clutter suppression allows for measurements of fragments of that portion of the front overlying severe clutter to the northeast. Overall, however, even in the severe Albuquerque clutter environment ASR-9 would detect a larger fraction of the total length of this front than would ASR-SS.

The weather images used for the simulations shown in Figures 18 through 23 feature high reflectivity components and strong spatial gradients. These illustrate the extent to which realistic pulse compression range sidelobes introduce artifacts in weather measurements under stressing scenarios. Figures 18 and 19 treat a Kansas City line storm with a strong reflectivity gradient and divergence line (large scale microburst) near its leading edge. The figures assume, respectively, -55 dB and -40 dB range sidelobes for ASR-SS. Comparison of the input and simulated images shows some areas where the range sidelobes produce observable "ghosting" (e.g., west and southwest of the radar on the leading edge of the line). For the less favorable range-sidelobe case of Figure 19, maximum reflectivity for the artifacts is 25 dBZ, above the level one precipitation intensity threshold. The velocity fields would appear largely unaltered using the solid-state transmitter; the most obvious effect is truncation of the leading edge of the outflow where it is within the 12 km range circle of reduced sensitivity.

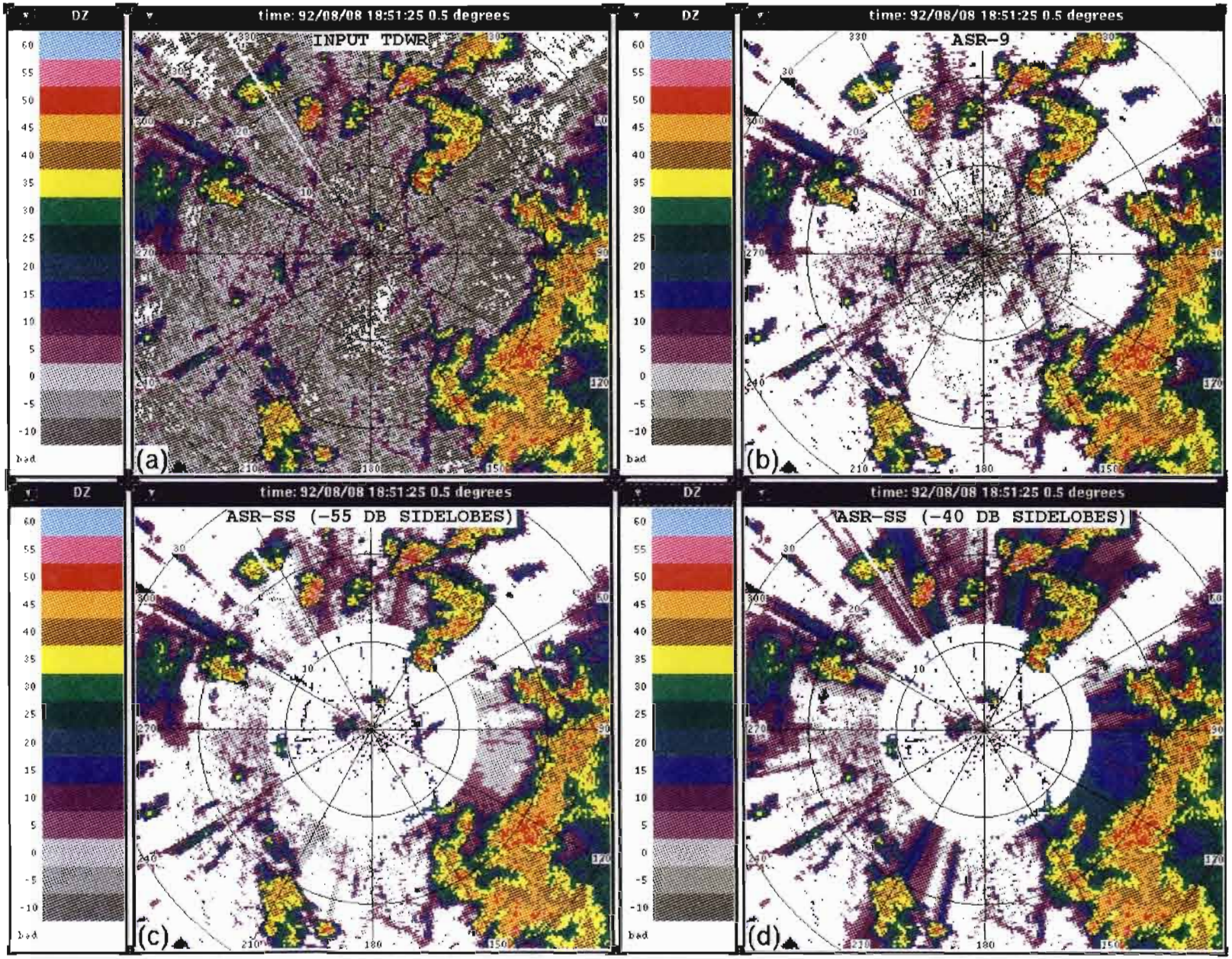

Figure 14. Comparative simulations of gust front thin lines measured by ASR-9 and ASR-SS. Panel (a) shows input reflectivity image from TDWR testbed in Orlando. Panel (b) simulates ASR-9 measurement by deleting resolution cells where ASR-9's SNR would not exceed 5 dB. Simulations for ASR-SS are shown in panels (c) and (d) assuming -55 and -40 dB peak range sidelobes.

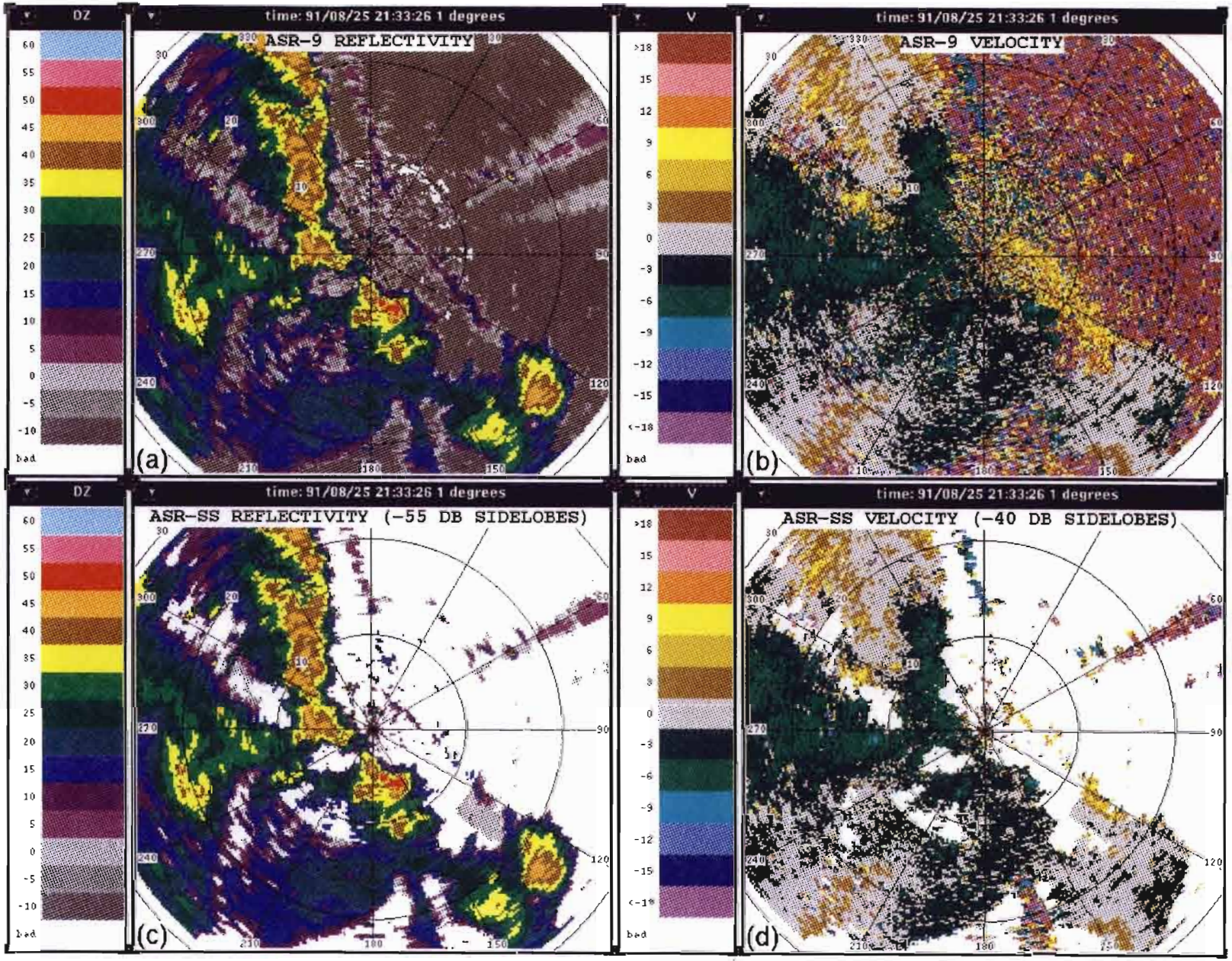

Figure 15. Simulation of gust front thin line measurements by ASR-SS. Panels (a) and (b) are reflectivity and Doppler velocity measurements from ASR-9 testbed in Orlando. ASR-SS measurements are simulated in panels (c) and (d), assuming -55 dB and -40 dB peak range sidelobes, respectively.

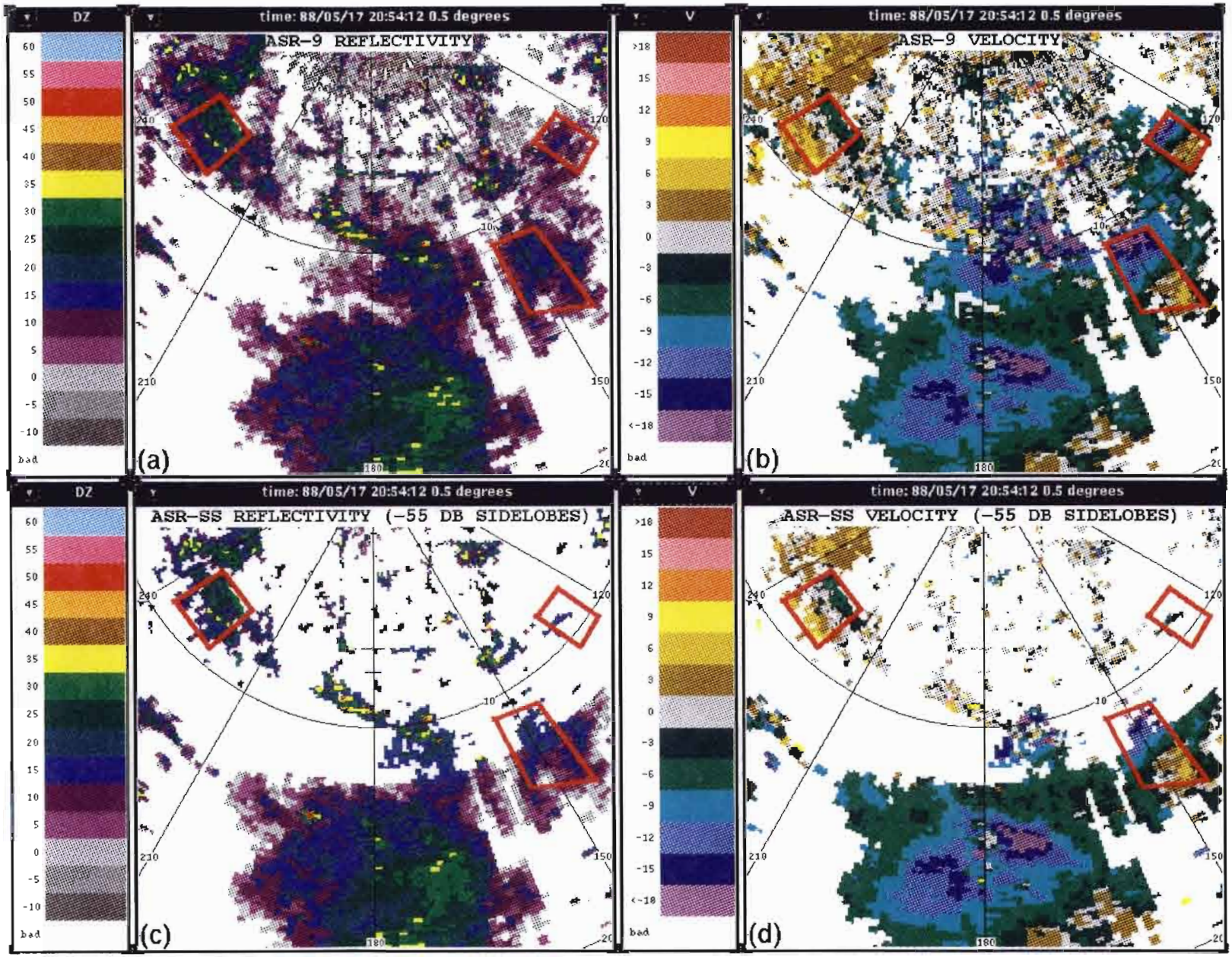

Figure 16. Comparative simulations of dry microbursts measured by ASR-9 and ASR-SS. Input data for the simulation are from TDWR testbed in Denver. Panels (a) and (b) simulate ASR-9 reflectivity and radial velocity measurements. Negative velocities denote flow towards the radar, and red outlines show locations of microburst divergent outflows. Panels (c) and (d) simulate ASR-SS measurements. Peak range sidelobes of -55 dB are assumed.

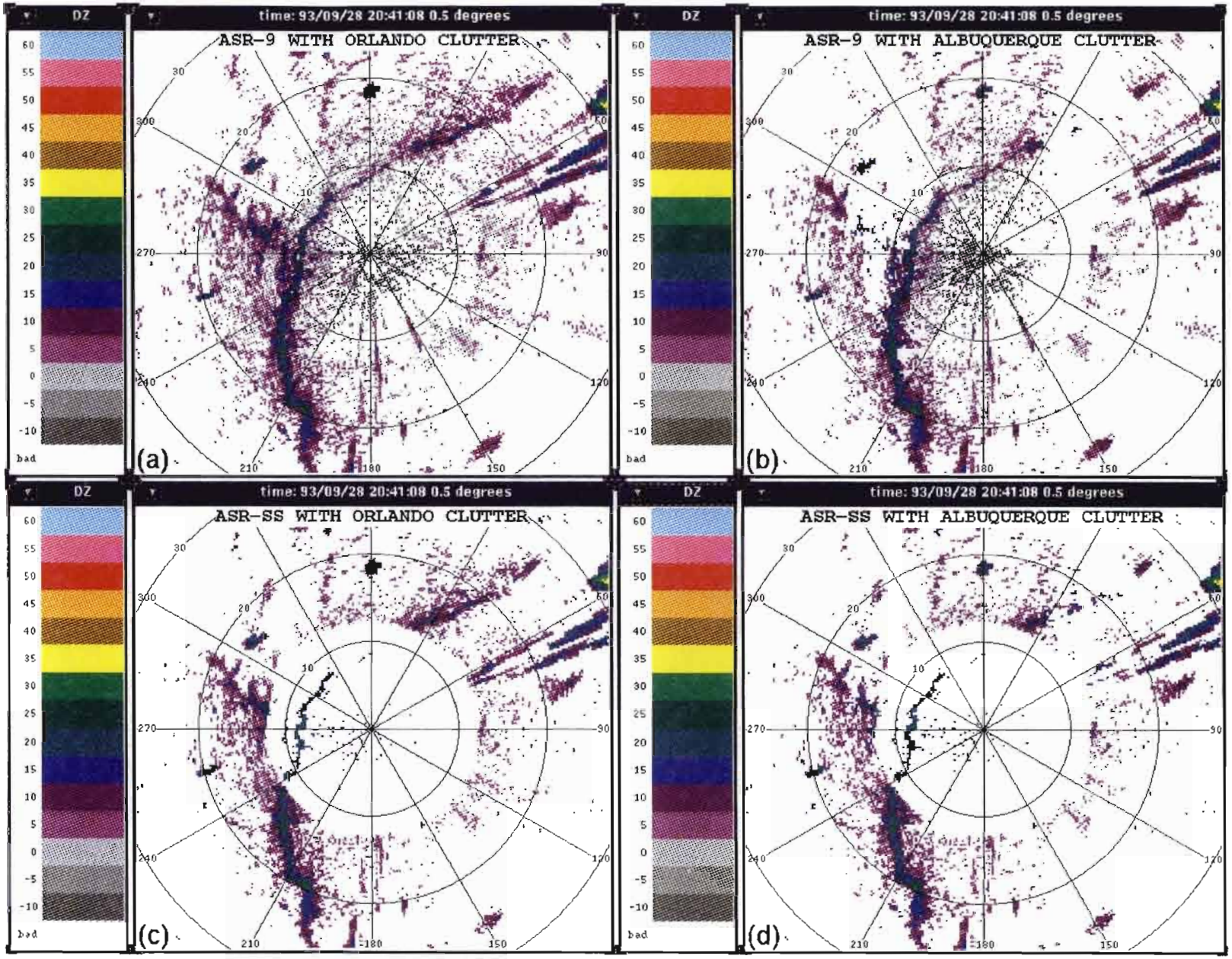

Figure 17. Comparative simulations of gust front thin line measured by ASR-9 and ASR-SS. Input data for the simulation are from TDWR testbed in Orlando. Panels (a) and (b) simulate ASR-9 reflectivity measurement in moderate (Orlando) and severe (Albuquerque) ground clutter environments. Panels (c) and (d) are corresponding simulations for ASR-SS. Peak range sidelobes of -55 dB are assumed.

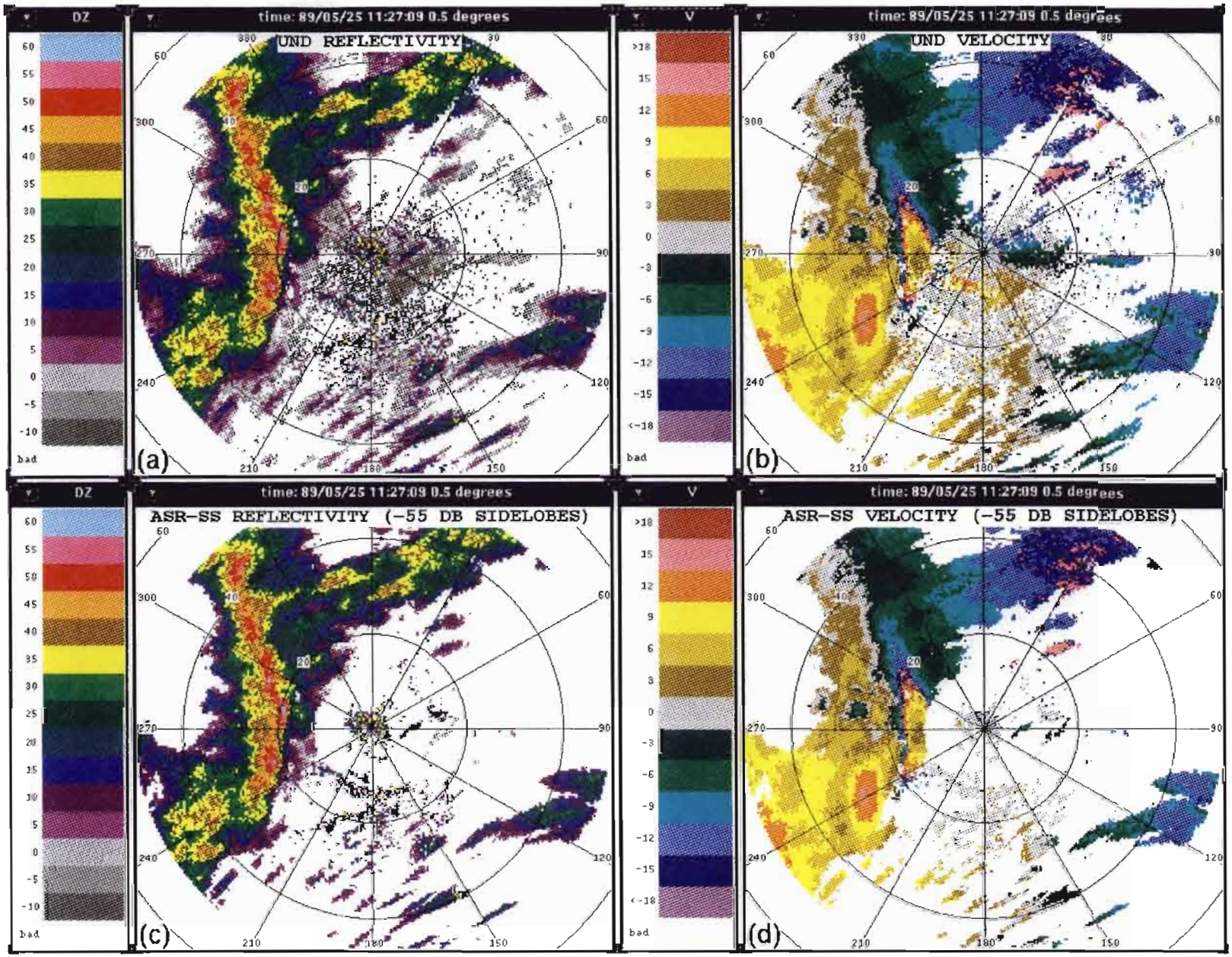

Figure 18. Simulated ASR-SS measurement of Kansas City squall line. Panels (a) and (b) are reflectivity and Doppler velocity images measured with the University of North Dakota (UND) radar. Panels (c) and (d) are solid state transmitter simulations assuming -55 dB peak range sidelobes.

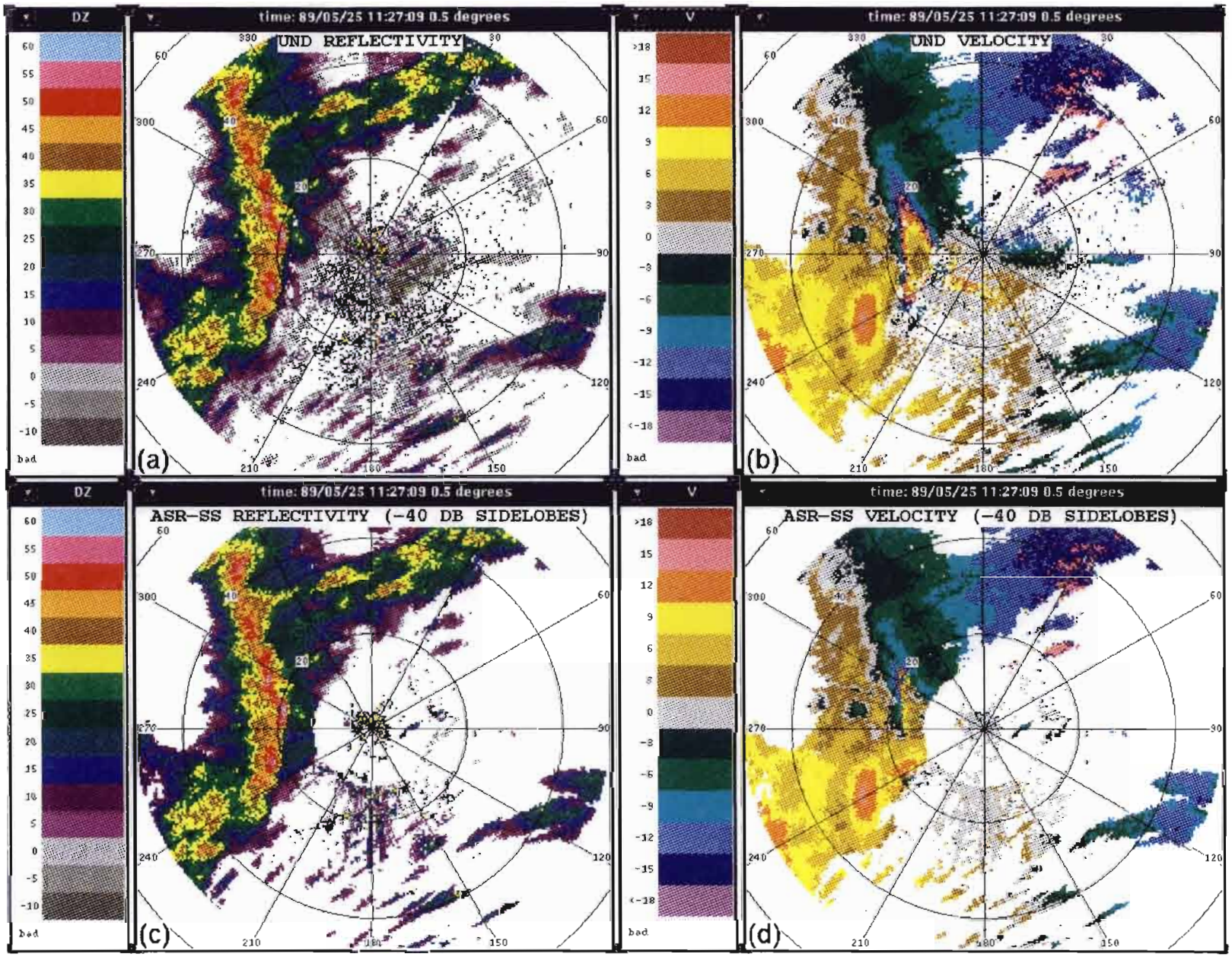

Figure 19. Simulated ASR-SS measurement of Kansas City squall line as in Figure 18, except that -40 dB peak range sidelobes are assumed.

Corresponding simulations of an Orlando hail storm case are shown in Figures 20 and 21. With the -55 dB peak range sidelobes (Figure 20), spokes of 5-10 dBZ false weather are produced extending approximately 10 km in advance of the storm. These mimic a gust front thin line echo and could result in a false wind shift warning. (Coincidentally, in this case there was an actual gust front in the vicinity of the false weather line in front of the storm.) For the -40 dB peak sidelobe simulation in Figure 21, a pedestal of 10-25 dBZ false reflectivity extends both in front of and behind the actual storm. This exceeds the level one threshold over a significant area. A six-level depiction of the data (panel d) gives the erroneous impression that a more extensive stratiform rain shield surrounds the hail storm.

Figures 22 and 23 treat another Orlando hailstorm, again exhibiting very high maximum reflectivity and a sharp reflectivity gradient at the storm's leading edge. As in the preceding case, the range sidelobes of ASR-SS result in noticeable ghosting in the echo free region ahead of the storm (e.g., 300° - 360° azimuth, 12-20 km range). In the -55 dB sidelobe simulation (Figure 21), the associated reflectivity is low so that in a six-level representation (panels (b) and (d)) the false weather is evident only in a very small region 20 km north of the radar. For the -40 dB sidelobe simulation, the false reflectivity indications exceed the level one or level two thresholds over a significant area in advance of the storm.

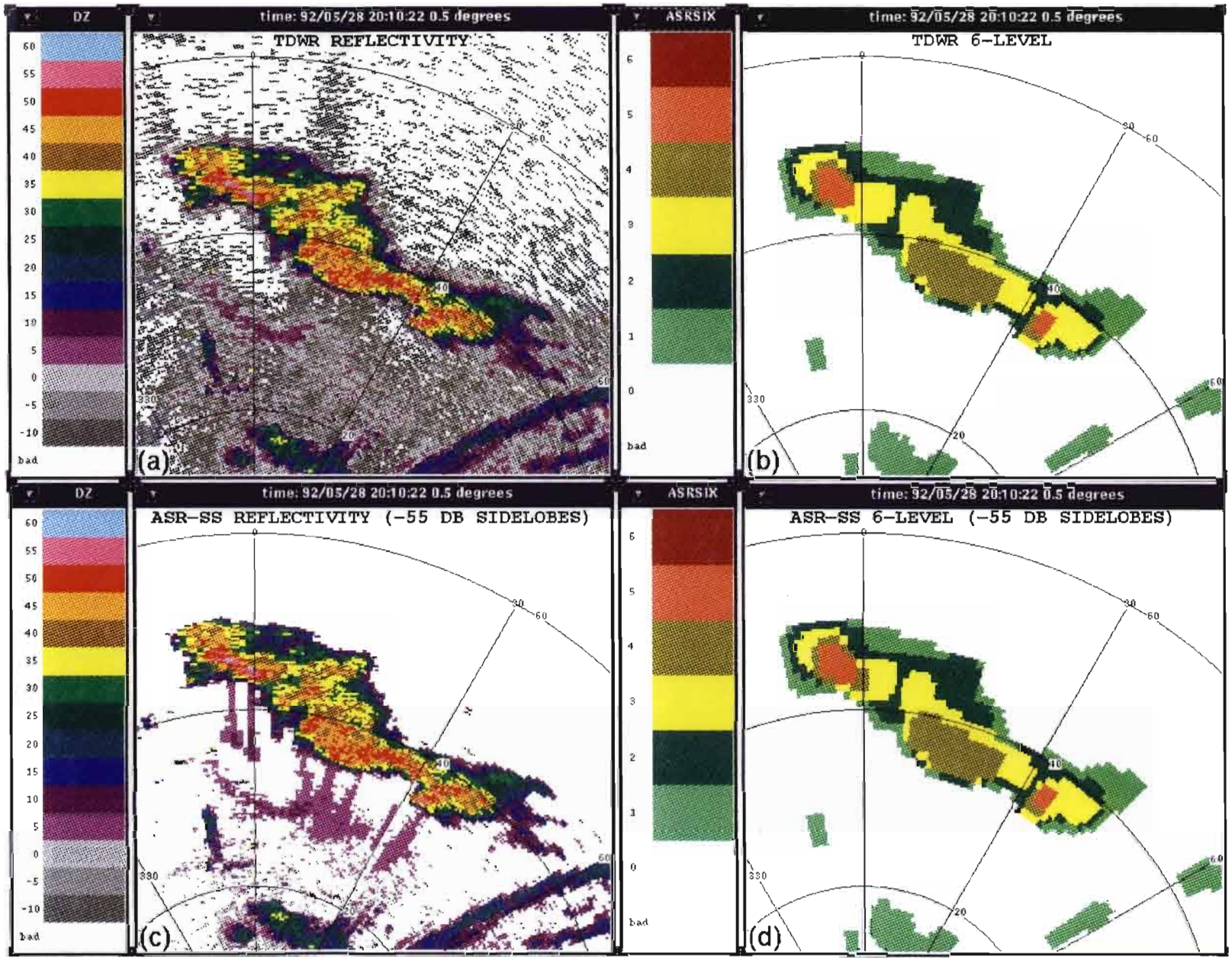

Figure 20. Simulated ASR-SS measurement of Orlando hail storm on 28 May, 1992. Panels (a) and (b) are reflectivity measurements from TDWR testbed. In (b) these are quantized according to six NWS levels of Table 1, after spatial smoothing such as employed by ASR-9 six-level weather processor. Panels (c) are (d) are corresponding output of ASR-SS, simulated assuming -55 dB peak range sidelobes.

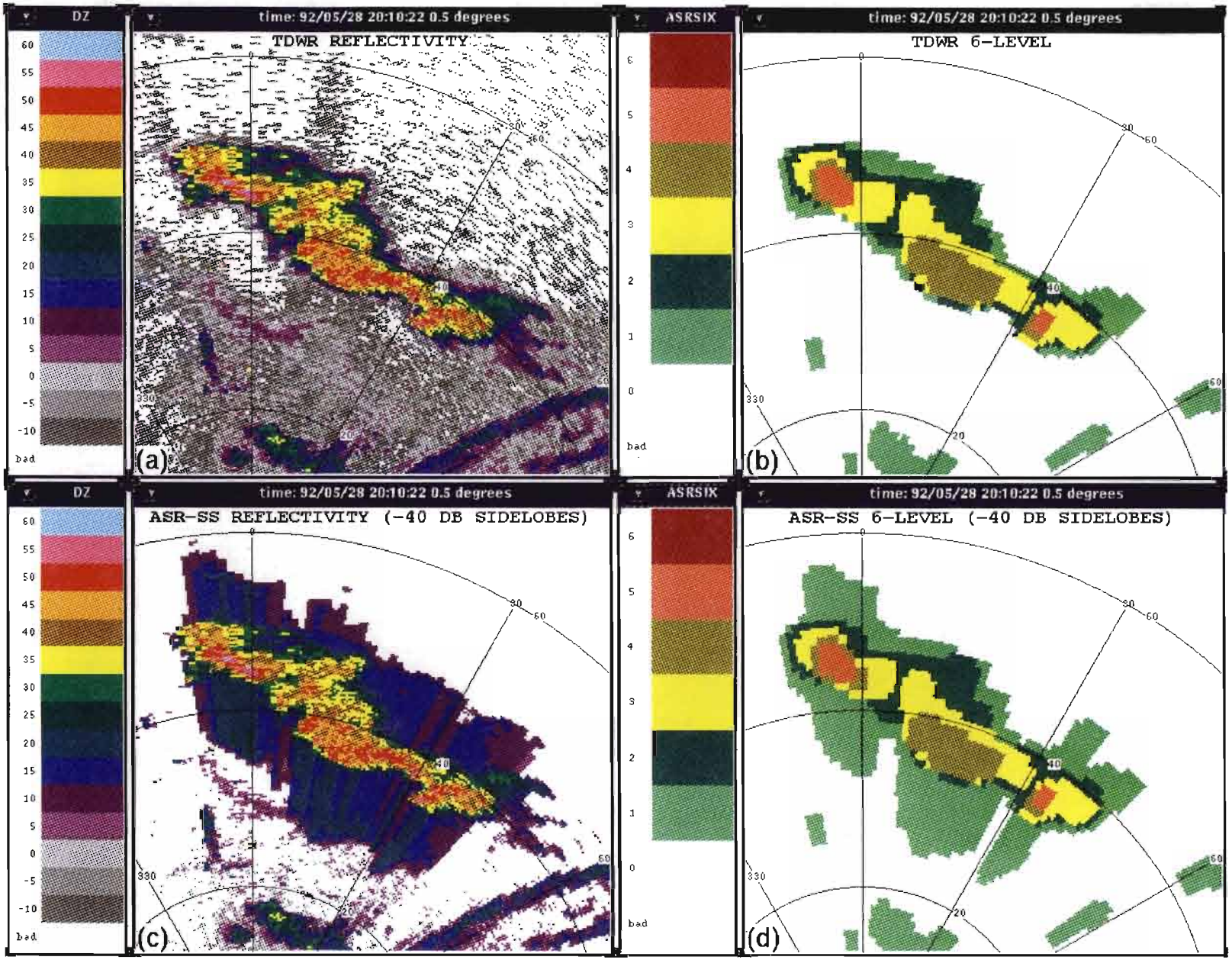

Figure 21. Simulated ASR-SS measurement of Orlando hail storm on 28 May, 1992 except that ASR-SS simulations in panels (c) and (d) assume -40 dB peak range sidelobes.

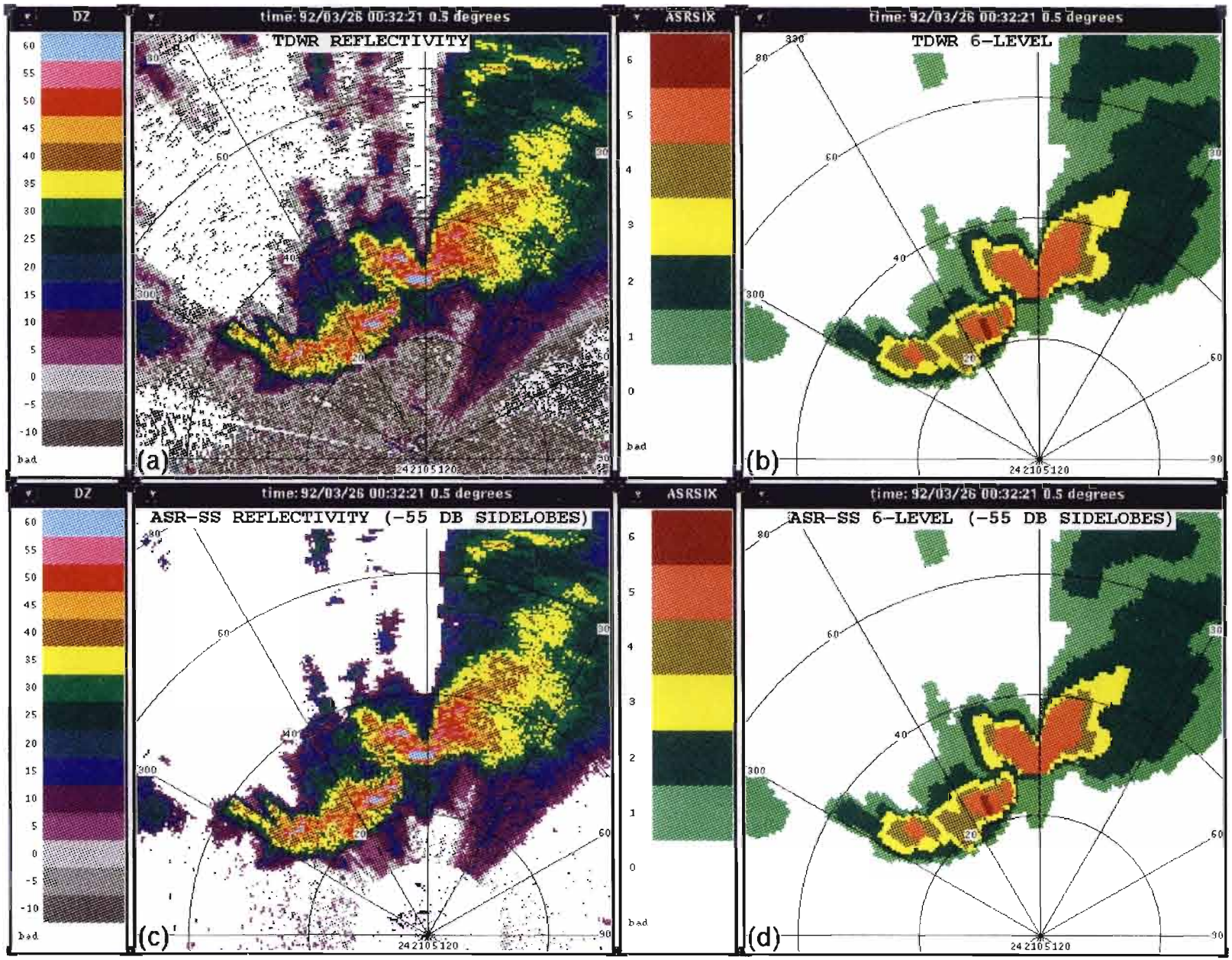

Figure 22. Simulated ASR-SS measurement of Orlando hail storm on 26 March, 1992. Input reflectivity measurements from TDWR testbed are shown in panels (a) and (b) in dBz and "six-level" units. Corresponding images from ASR-SS are simulated in (c) and (d) assuming -55 dB peak range sidelobes.

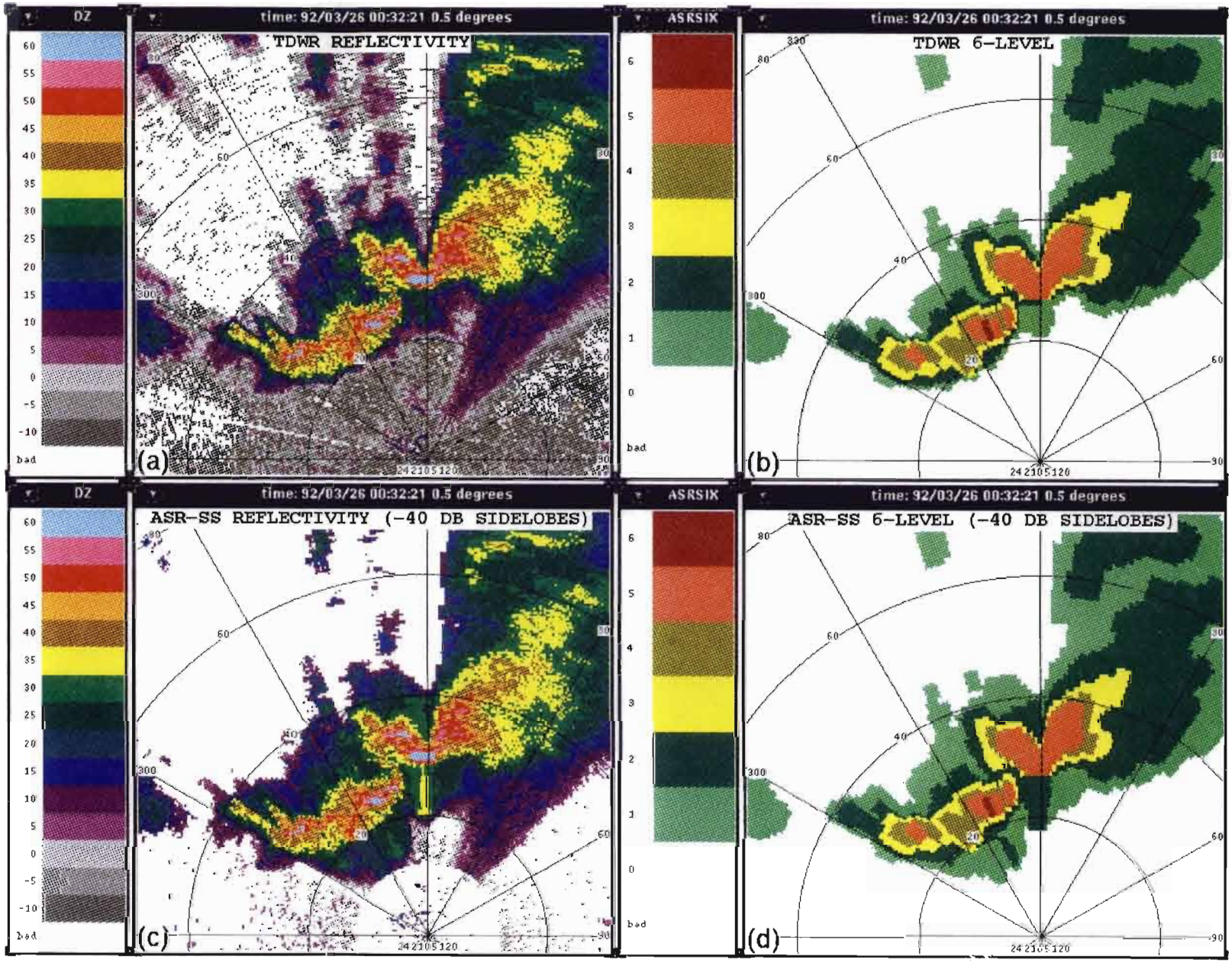

Figure 23. Simulated ASR-SS measurement of Orlando hail storm on 26 March, 1992 except that ASR-SS simulations in panels (c) and (d) assume -40 dB peak range sidelobes.

7. SUMMARY AND DISCUSSION

These analyses and simulations indicate that a suitably designed ASR-11 with solid state transmitter could support six-level weather reflectivity measurement with minimal degradation relative to what is achieved with ASR-9. System sensitivity and clutter suppression capability are more than adequate to measure weather with reflectivity exceeding the 18 dBZ threshold for "level one"–the lowest displayed precipitation intensity level. In the storm cases simulated, range sidelobes maintained at -55 dB did not produce significant artifacts exceeding this 18 dBZ threshold. More noticeable level one and level two reflectivity artifacts were generated in simulations that assumed -40 dB peak range sidelobes. In a few of the simulations, these were of sufficient spatial extent that they might alter operational decision making in an ATC environment.

A solid state transmitter ASR-11's ability to support microburst and gust front detection is considerably more problematic, owing to the lower radar cross section that may be associated with wind shear phenomena. Our analyses indicate that reduced sensitivity in the short range interval where a low peak power uncompressed pulse must be used is a significant impediment to gust front detection and to microburst detection in those environments where "dry" microbursts are prevalent. The improved clutter suppression capability of a solid state transmitter does not offset this loss of sensitivity. Overall, our analyses suggest that the fraction of low cross section wind shear phenomena detectable by ASR-SS would be roughly one quarter to one-third smaller than with the ASR-9. Finally, false weather echoes caused by pulse-compression range sidelobes may occur at a reflectivity level comparable with some wind shear phenomena. Our simulations showed an example of range-sidelobe artifacts that mimic a gust front thin line and could produce a false alarm were these data being processed by an automated gust front detection algorithm.

These analyses and simulations do, of course, have a number of limitations. As noted, the actual clutter suppression capability of a solid state transmitter ASR may not be limited solely by transmitter instability. It is likely therefore that we have somewhat overestimated the capability of such a radar to measure weather in the presence of ground clutter. A more significant issue is accurate treatment of the capability to detect subtle wind shear signatures, such as gust front thin lines, at low signal-to-noise or signal-to-clutter residue ratios. The approach we have adopted for detecting such signatures using the ASR-9 WSP is to run the signal processor without signal-to-noise or clutter-residue thresholding; this maximizes the likelihood that signatures will be present in the imagery input to the detection algorithm. Weather parameter estimates at low SNR and/or low signal-to-clutter ratio are extremely dependent on details of the weather, clutter and noise spectrum and on the processing algorithms used to estimate these parameters. Accurate modeling of these effects is difficult.

Finally, owing to proprietary considerations, we do not have detailed understanding of the long-pulse waveform used as the basis for the ASR-SS simulations nor of the processing that is used to compensate for non-ideal transmitter/receiver characteristics. While simulations based on the (known) ambiguity function should adequately account for the major effects of range-Doppler sidelobes, there may be subtle second-level effects not accounted for.

Overall, however, we believe that these analyses are adequate to confirm the suitability of a solid state transmitter ASR-11 for providing six-level weather reflectivity information, provided that peak range sidelobes are maintained at approximately -55 dB. They also clearly indicate that the capability of such a radar to detect subtle wind shear phenomena would be degraded relative to that of the ASR-9, with the issue of reduced short-range sensitivity the largest concern. Full understanding of the impact here can probably not be resolved through simulation. Acquisition of data sets with real weather and clutter signals would be necessary to fine tune the algorithms to match the capabilities and limitations of the solid-state system.

REFERENCES

1. M.E. Weber and T.A. Noyes, "Wind Shear Detection with Airport Surveillance Radars," *Lincoln Laboratory Journal*, 3, 511-526, 1989.

2. T.A. Healy and R.L. Ferranti, "ASR Solid State Transmitter Demonstration Final Report," FAA Technical Center, Atlantic City Airport, NJ, 1993.

3. M.E. Weber and W.R. Moser, "A Preliminary Assessment of Thunderstorm Outflow Wind Measurement with Airport Surveillance Radars," Lincoln Laboratory Project Report ATC-140, FAA-PM-86-38, 1987.

4. M.E. Weber, "Dual-Beam Autocorrelation Based Wind Estimates from Airport Surveillance Radar Signals," Lincoln Laboratory Project Report ATC-167, FAA-PS-89-5, 1989.

5. R.L. Delanoy and S.W. Troxel, "Machine Intelligent Gust Front Detection," *Lincoln Laboratory Journal*, 6, 187-212, 1993.

6. D. Klingle-Wilson and M.F. Donovan, "Characteristics of Gust Fronts," Preprint Volume: *Fourth International Conference on Aviation Weather Systems*, June 24-28, 1991, Paris, France. Published by the American Meteorological Society, Boston, MA.

7. M.E. Weber, "Ground Clutter Processing for Wind Measurements with Airport Surveillance Radars," Lincoln Laboratory Project Report ATC-143, FAA-PM-87-21, 1987.

APPENDIX A.
SIMULATION OF WEATHER IMAGES FROM A SOLID STATE TRANSMITTER RADAR USING PULSE COMPRESSION

Denote the uncompressed pulse waveform as *s(t)* which is transmitted over the interval -T/2 < t < T/2. The echo received from a discrete target is a scaled, Doppler shifted version of the transmitted waveform:

$$e(t)=a\, s(\delta_{\upsilon}[t-\tau]) \tag{A-1}$$

where $\tau = 2R / c$ is proportional to the range of the target, δ_{υ} is the "time compression factor" associated with the target's Doppler velocity υ and amplitude a accounts for target cross section and signal propagation loss. The output of a pulse compression receiver at time η is:

$$r(\eta)=\int_{-T/2}^{T/2} s^*(t')e(t'+\eta)dt' \tag{A-2}$$

$$=a\int_{-T/2}^{T/2} s^*(t')s(\delta_{\upsilon}[t'+\eta-\tau])dt'$$

$$=aH(\upsilon,\eta-\tau)$$

where $H(\upsilon,\tau)$ is the cross-correlation of the signal and its Doppler shifted replica evaluated at velocity υ and delay τ. The magnitude squared of this function is the signal "ambiguity function."

We model weather as a distributed target which returns a signal with (complex) range and Doppler spectrum $a(\tau,\upsilon)$. The output of the pulse-compression receiver is now:

$$r(\eta)=\int_{\eta-T}^{\eta+T} d\tau\int d\upsilon\, a(\tau,\upsilon)H(\upsilon,\eta-\tau) \tag{A-3}$$

Weather reflectivity as measured with the pulse compression receiver is:

$$\hat{Z}(\eta)=K\eta^2<r^*(\eta)r(\eta)> \tag{A-4}$$

$$= K\eta^2 < \int_{\eta-T}^{\eta+T} d\tau \int d\upsilon\, a^*(\tau,\upsilon) H^*(\upsilon,\eta-\tau) \int_{\eta-T}^{\eta+T} d\tau' \int d\upsilon'\, a(\tau',\upsilon') H(\upsilon',\eta-\tau') >$$

$$= K\eta^2 \int_{\eta-T}^{\eta+T} d\tau \int d\upsilon <|a(\tau,\upsilon)|^2> |H(\upsilon,\eta-\tau)|^2$$

We can relate this to the actual distribution of weather reflectivity, $Z(\tau)$ by assuming that the ambiguity function is independent of Doppler velocity and that:

$$Z(\tau) = K\tau^2 \int d\upsilon <|a(\tau,\upsilon)|^2> \tag{A-5}$$

Thus:

$$\hat{Z}(\eta) = \eta^2 \int_{\eta-T}^{\eta+T} d\tau \frac{Z(\tau)\,|H(\upsilon,\eta-\tau)|^2}{\tau^2} \tag{A-6}$$

Similarly, it can be shown that the mean Doppler velocity measured using a pulse compression receiver is:

$$\hat{\upsilon}(\eta) = \frac{\int_{\eta-T}^{\eta+T} d\tau \frac{Z(\tau)\,\upsilon(\tau)\,|H(\upsilon,\eta-\tau)|^2}{\tau^2}}{\int_{\eta-T}^{\eta+T} d\tau \frac{Z(\tau)\,|H(\upsilon,\eta-\tau)|^2}{\tau^2}} \tag{A-7}$$

where $\upsilon(\tau)$ is the actual distribution of Doppler velocity in range.

Range sidelobe structures used for the simulations in Section 6 are plotted in Figure A-1. The upper plot shows a simplified version of the sidelobe structure of the solid state transmitter/receiver system tested with an ASR-9 at the FAA Technical Center. Peak range sidelobes are -55 dB and are taken as invariant with target Doppler over the +/- 50 m/s interval of concern for weather surveillance. In the lower plot, we raise the peak sidelobes to -40 dB.

Weather reflectivity and Doppler velocity images measured by the ASR-WSP and TDWR testbeds were used as "true" distributions of the weather spectrum moments. At ranges greater than 12 km, these are "filtered" along the range axis using the kernels defined in equations (A-6) or (A-7) to simulate the effects of the pulse-compression range sidelobes. Clutter measurements obtained with the ASR-9 testbed in Orlando and Albuquerque were used to calculate clutter residue. These represent, respectively, moderate and severe clutter environments. Data values for resolution cells where reflectivity does not exceed the equivalent reflectivity of system noise (see Figure 2) by 5 dB, and that of clutter residue by at least 10 dB, are then removed from the image to account for the sensitivity and clutter suppression limits of the solid state system. The 5 dB SNR requirement was chosen as intermediate between the requirements for microburst and gust front thin line measurement described in Section 3.

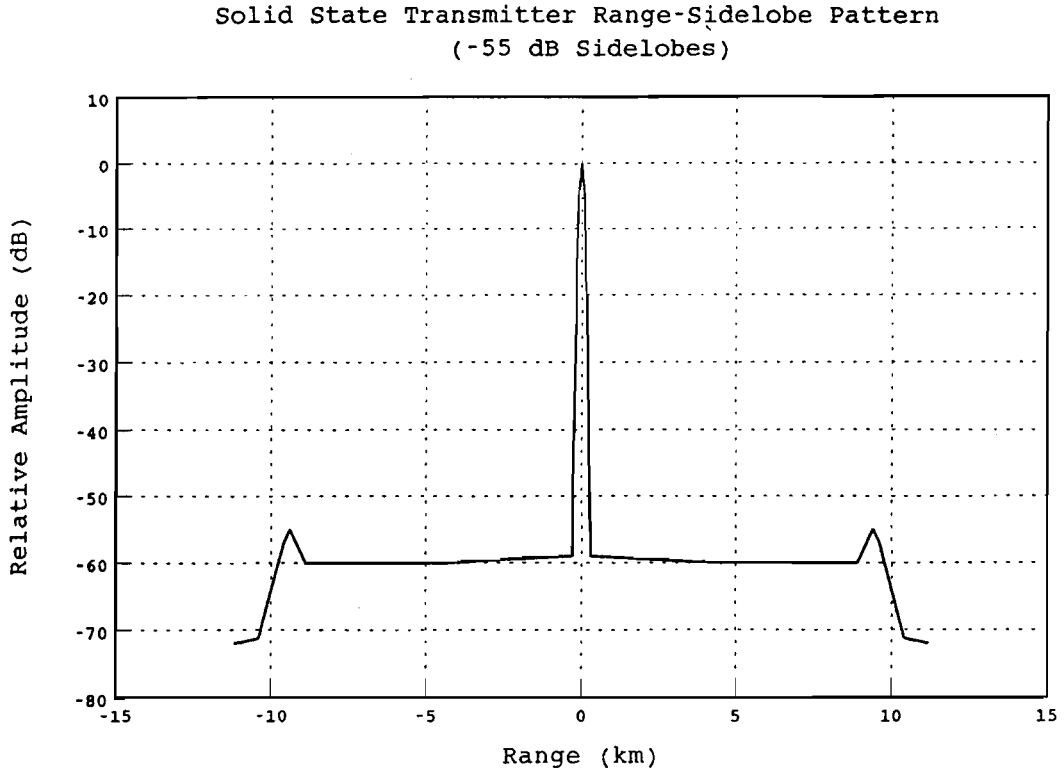

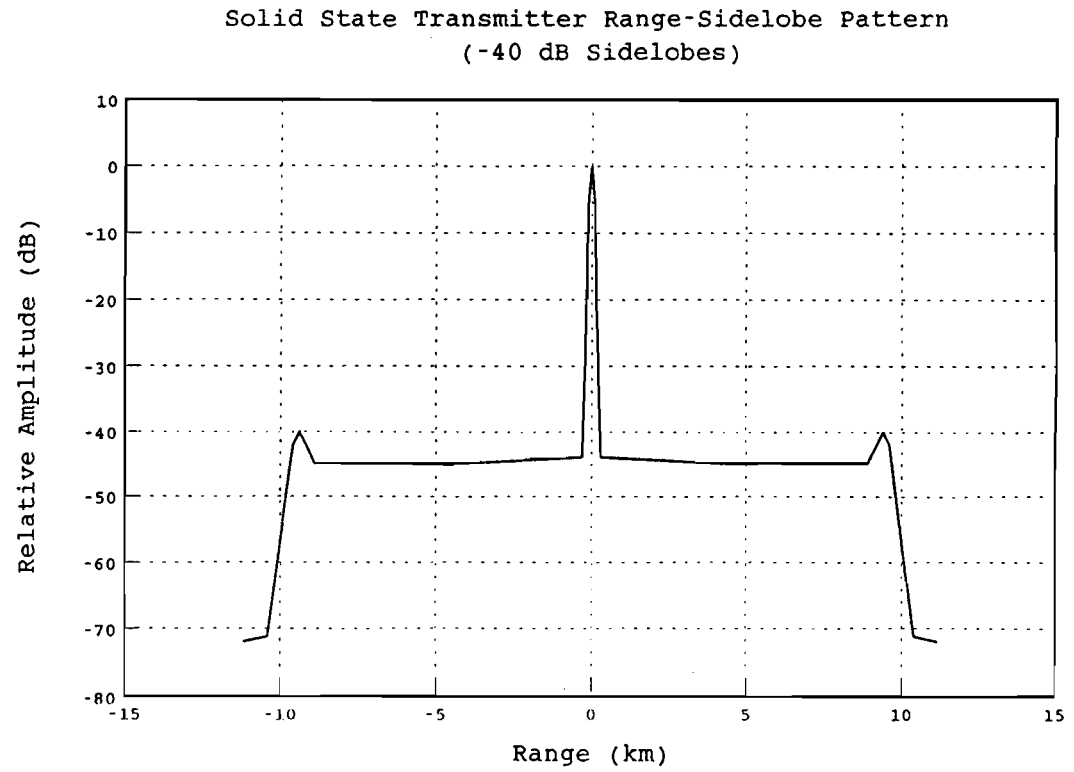

Figure A-1. Range sidelobe structures assumed for the simulations in Section 6. Peak sidelobes are taken as -55 dB (upper panel) and -40 dB (lower panel).

ACRONYMS AND ABBREVIATIONS

AAS	Advanced Automation System
AGC	Automatic Gain Control
ATC	Air Traffic Control
FAA	Federal Aviation Administration
FAATC	Federal Aviation Administration Technical Center
MIGFA	Machine Intelligent Gust Front Algorithm
NAS	National Airspace System
NDI	Non-Developmental Item
NWS	National Weather Service
ORD	Operational Requirements Document
PPI	Plan Position Indicator
PRI	Pulse Repetition Interval
RMMS	Remote Maintenance Monitoring System
SNR	Signal-to-Noise Ratio
STC	Sensitivity Time Control
TASS	Terminal Area Surveillance System
TDWR	Terminal Doppler Weather Radar
UND	University of North Dakota
WSP	Wind Shear Processor